A global analysis of reconstructed land climate changes during Dansgaard-Oeschger events

Mengmeng Liu[1,2,*], Iain Colin Prentice[1], Sandy P. Harrison[2]

1: Georgina Mace Centre for the Living Planet, Department of Life Sciences, Imperial College London, Silwood Park Campus, Buckhurst Road, Ascot SL5 7PY, UK

2: Department of Geography and Environmental Science, University of Reading, Reading, RG6 6AB, UK

*** Corresponding author: Mengmeng Liu (m.liu18@imperial.ac.uk)**

Ms for: *Climate of the Past*

Abstract

Dansgaard–Oeschger (D–O) warming events are comparable in magnitude and rate to the anticipated 21st century warming. As such, they provide a good target for evaluation of the ability of state-of-the-art climate models to simulate rapid climate changes. Despite the wealth of qualitative information about climate changes during the D-O events, there has been no attempt to date to make quantitative reconstructions globally. Here we provide reconstructed changes ~~ions~~ of seasonal temperature ~~change~~s and ~~changes in~~ plant-available moisture across multiple D-O events ~~during~~ between 50 and 30 ka ~~Marine Isotope Stage 3~~ based on available pollen records across the globe. These reconstructions show that the largest warming occurred in northern extratropics, especially Eurasia, while western North America and the southern extratropics were characterised by cooling. The change in winter temperature was significantly larger than the change in summer temperature in the northern extratropics and the tropics, indicating that the D-O warming events were characterised by reduced seasonality, but there was no significant difference between the summer and winter temperature changes in the southern extratropics. The antiphasing between northern and southern extratropical changes, and the west-east pattern of cooling and warming in North America were generally consistent across the eight D-O events examined, although coherency is greatest during the strongest events. There was no globally consistent pattern between changes in moisture and changes in temperature. ~~The change in winter temperature was significantly larger than the change in summer temperature in the northern extratropics, indicating that the D-O warming events were~~

~~characterised by reduced seasonality, but there is no significant difference between the summer and winter temperature changes in the southern extratropics. The antiphasing between northern and southern extratropical changes, and the west-east pattern of cooling and warming in North America are consistent across the eight D-O events examined, although the signal at individual sites may vary between events. Globally, changes in moisture were positively correlated with changes in temperature, but the strength and the sign of this relationship vary regionally.~~ These reconstructions can be used to evaluate the spatial patterns of changes in temperature and moisture in the transient simulations of the D-O events planned as part of the Palaeoclimate Modelling Intercomparison Project.

1. Introduction

Dansgaard–Oeschger (D–O) events are characterised in Greenland by a transition from cold Greenland Stadial (GS) to warmer Greenland Interstadial (GI) conditions (Dansgaard et al., 1993). The surface air temperature in Greenland increased by 10–16~~5~~° C during the warming phases; these warming events occurred over an interval of between 50 and 200 years (Huber et al., 2006; Kindler et al., 2014). Thus, the D-O events offer a parallel in terms of speed to projected future warming, although both the baseline state and the mechanism inducing this warming differ from anticipated 21st century climate changes. D-O events could therefore provide an opportunity to determine how well climate models that are used for future projections can simulate rapid climate changes (Malmierca-Vallet et al., 2023), particularly regional patterns of warming (and cooling) that are regarded as a challenge for modelling (Doblas-Reyes et al., 2021; Lee et al., 2021) and are highly important in assessing the vulnerability of human societies to future climate changes (IPCC, 2022).

Although D-O events are found throughout the last glacial period, the largest number and the most regular patterning occurred during Marine Isotope Stage 3 (MIS 3; 57 to 29 ka) when there were 11 separate events (D-O 15 to D-O 5), while earlier stage such as MIS 4 (71 to 57 ka) only had 3 separate events (D-O 18 to 16). The typical duration of a cycle as manifested in Greenland is *ca.* 1500 years and is characterised by an initial short slow warming, followed by an abrupt large warming in matter of decades, followed by a long slow cooling over centuries to millennia, with a terminal phase of fast cooling (e.g. D-O 8, D-O 12). However, there are also cycles in which the warming and cooling phases took roughly the same time (e.g. D-O 5, D-O 6, D-O 9). The magnitude of changes also differ, with both strong events (e.g. D-O 8, D-O 12) and weak events (e.g. D-O 9).

The D-O signals are not just in Greenland – they are registered globally

~~D-O events are registered globally~~ (Adolphi et al., 2018; Corrick et al., 2020; Harrison and Sanchez-Goñi, 2010; Sánchez-Goñi et al., 2017; Voelker, 2002) ~~.~~ and are reflected in changes in both temperature and precipitation. Both oceanic and ice-core records indicate that temperature changes are out-of-phase between the northern and southern hemispheres, and the southern hemisphere response both in terms of warming and cooling phases is generally less abrupt (Dima et al., 2018; Vettoretti and Peltier, 2015). There is a comparative lack of information from the continents about the manifestation of D-O events. Shifts in vegetation

types between GI and GS states have been interpreted as primarily a temperature signal in the extratropics and a moisture signal in the tropics (Harrison and Sanchez-Goñi, 2010). Speleothem records provide a good time-control on the synchroneity of climate changes globally with the D-O events registered in Greenland (Adolphi et al., 2018; Corrick et al., 2020), but the driver of this signal can either be temperature or precipitation depending on the region. There are quantitative climate reconstructions based on terrestrial pollen records from La Grande Pile (Guiot et al., 1993), Lago Grande di Monticchio (Huntley et al., 1999), Padul (Camuera et al., 2022), El Cañizar de Villarquemado (Camuera et al., 2022; Wei et al., 2021) and Lake Ohrid (Sinopoli et al., 2019), marine cores in the western Mediterranean and offshore from Portugal (Sánchez-Goñi et al., 2002), diatom assemblages at Les Echets, France (Ampel et al., 2010), chironomids from Lake Bergsee in central Europe (Lapellegerie et al., 2024), bacterial membrane lipid records from the Eifel region (Zander et al., 2024), isotopic measurements of earthworm calcite from the Rhine Valley (Prud'homme et al., 2022) and clumped isotope measurements on snails in Hungary (Újvári et al., 2021). Aside from the lack of comparable quantitative estimates from outside Europe, differences in the methodology employed and in the specific climate variables reconstructed in each of these studies limits their usefulness for model evaluation. In particular, given that there is still uncertainty as to whether the D-O cycles are characterised by changes in seasonality such that warming events are primarily driven by changes in winter (Flückiger et al., 2008; Zander et al., 2024; Zumaque et al., 2025), in the regional strength of the warming (Harrison and Sanchez-Goñi, 2010) and how warming relates to changes in moisture (Wei et al., 2021), there is a need for more systematic reconstruction of seasonal climate changes.

In the paper, we provide reconstructed changes in~~ions of~~ seasonal temperatures ~~changes~~ and ~~changes in~~ plant-available moisture during the intervals corresponding to D-O warming events in Greenland between 50 and 30 ka ~~during Marine Isotope Stage 3~~ based on available pollen records globally. We use ~~employ a standard methodology to construct age models for these records, as well as~~ a standard regression-based approach to make the reconstructions. We analyse the regional patterns to identify key targets for model evaluation.

2. Methods

2.1. Data sources

Modern pollen data were obtained from version 3 of the SPECIAL Modern Pollen Dataset (SMPDSv3) (Harrison et al., 2025a). This global dataset was constructed by amalgamating and standardising records from public repositories (e.g. Neotoma, Pangaea), existing regional databases (e.g. European Modern Pollen Database, African Pollen Database), individual publications and records provided by the original authors. The records were carefully screened to remove duplicates that were present in more than one source. The modern samples were obtained from multiple types of record, including pollen traps, surface samples, moss polsters and different types of sediment, including cores from lakes and peatbogs, and section through e.g. fluvial or loess deposits. In cases where the record was radiometrically dated, the database preserves all samples younger than 50 yr B.P. However, some samples were undated and are therefore recorded as modern if a collection date was given or assumed modern if not.

~~This global~~The dataset contains 26704~~26489~~ samples from 18202~~18086~~ different locations, and ~~. The dataset~~ was created after removing taxa that are not climatically diagnostic (e.g. obligate aquatics, carnivorous species, cultivated plants). The dataset provides several levels of taxonomic aggregation; here we use the most aggregated level, where woody species were generally combined at genus level and herbaceous species at sub-family or family level unless they were palynologically distinctive, occupied distinctive ecological niches and were sufficiently geographically widespread. This "amalgamated" dataset contains relative abundance information for 1367~~1362~~ taxa. These samples were aggregated by location (which is longitude, latitude and elevation) in order to remove duplicates. Counts for *Quercus*, *Quercus* (deciduous) and *Quercus* (evergreen) were combined because of inconsistent differentiation of *Quercus* pollen in different regional records. Deciduous and evergreen oaks occupy different areas of climate space, particularly in terms of seasonal moisture; specifically, evergreen oaks are typically found in areas characterised by winter rainfall such as the Mediterranean. Nevertheless, since there are other plant taxa that are similarly diagnostic of such regimes, the amalgamation of *Quercus* (deciduous) and *Quercus* (evergreen) should not have a major effect on the robustness of our climate reconstructions. We have tested this assumption by making reconstructions based on all taxa except *Quercus* (Supplementary Materials, ~~Section~~ section 4). Taxa that occurred in less than 10 samples in the training dataset were not used to make

reconstructions because it is unlikely that the available samples provided a reasonable estimate of the climate space occupied by these rare taxa (Liu et al., 2020). After the location aggregation and the taxa filter, the dataset contains information on 18202~~18086~~ samples with relative abundance information for 609~~607~~ taxa (Figure 1a).

We focus on three climate variables: mean temperature of the coldest month (MTCO), mean temperature of the warmest month (MTWA), and a plant-available moisture index (α_{plant}) defined as the estimated ratio of actual to equilibrium evapotranspiration. These three variables reflect ecophysiological controls on plant distribution (Harrison, 2020; Woodward, 1987) that have been shown to independently influence the distribution and abundance of plant species (Boucher-Lalonde et al., 2012; Wang et al., 2013; Wei et al., 2020). α_{plant} is a transformation of the commonly used moisture index MI (defined as the estimated ratio of annual precipitation to annual potential evapotranspiration) that emphasizes differences at the dry end of the climate range, which have a more pronounced effect on vegetation distribution than differences at the wet end (Prentice et al., 2017). Thus, α_{plant} can be better reconstructed from the pollen records than MI.

The climate values at each SMPDSv3 site were obtained using a geographically-weighted regression (GWR) of climatological values of mean monthly temperature, precipitation, and fractional sunshine hours from the Climatic Research Unit Time-Series version 4.04 (CRU TS4.04; Harris et al., 2020) dataset averaged over the period 1961–1990, which corresponds to the interval from which most of the pollen samples were derived. GWR was to correct for elevation differences between the CRU grid cells and the pollen sites. MTCO and MTWA were taken directly from the GWR. MI was calculated for each site using SPLASH v1.0 (Davis et al., 2017) based on daily values of precipitation, temperature and sunshine hours obtained using a mean-conserving interpolation of the monthly values of each. MI was then transformed to α_{plant} using the parametric Fu-Zhang formulation of the Budyko relationship (Supplementary Materials, section 2). T~~We have used a global pollen dataset for calibration of the pollen-climate relationships. The use of a global dataset, rather than region-specific training data, relies on the principle of phylogenetic niche conservatism (Harvey and Pagel, 1991; Qian and Ricklefs, 2004; Wang et al., 2025), which states that traits tend to remain constant over time and that the climatic niches of specific genera are also conservative (Harrison et al., 2025c). The use of a global dataset for calibration makes it possible to sample a large range of climates,~~

~~and thus makes it more likely that the reconstructions of glacial climates are realistic and not confined to the limited climate range sampled in any one region (Turner et al., 2020).~~

~~The SMPDSv3 also provides climatic information at each pollen site, specifically the mean temperature of the coldest month (MTCO), mean temperature of the warmest month (MTWA), and a plant-available moisture (α) calculated as the ratio of actual evapotranspiration to equilibrium evapotranspiration. These bioclimate variables reflect mechanistically distinct controls on plant growth. α is a transformation of the commonly used moisture index MI (Supplementary Materials, Section 2), to emphasize the differences at the dry end of the climate range, which have a more pronounced effect on vegetation distribution than differences at the wet end (Prentice et al., 2017). T~~he climate space occupied by SMPDSv3 (Figure S1) samples a reasonable range of global climate space and therefore should provide robust reconstructions of climate changes under glacial conditions.

We ~~have used~~use a global modern ~~pollen~~ dataset for calibration of the pollen-climate relationships. The use of a global dataset, rather than region-specific training data, relies on the principle of phylogenetic niche conservatism (Harvey and Pagel, 1991; Qian and Ricklefs, 2004; Wang et al., 2025), which states that traits tend to remain constant over time and that the climatic niches of specific genera are also conservative (Harrison et al., 2025c). The use of a global dataset for calibration makes it possible to sample a large range of climates, and thus makes it more likely that the reconstructions of glacial climates are realistic and not confined to the limited climate range sampled in any one region in modern times (Turner et al., 2020).

~~The fossil pollen data were obtained from the Abrupt Climate Changes and Environmental Responses (ACER) database (Sánchez-Goñi et al., 2017).~~ The Abrupt Climate Changes and Environmental Responses (ACER) database (Sánchez-Goñi et al., 2017) was originally created to provide a source of pollen and charcoal data for Marine Isotope Stage 3 (MIS 3), which includes 93 records ~~from the last glacial period (73-15 ka)~~ with sufficient resolution and dating control to detect sub-millennial scale variability. Much more records covering MIS 3 have become available since the compilation of the ACER database, such as the synthetic pollen databases available for Siberia (Cao et al., 2019, 2020) and China (Zhou et al., 2023) and the global Legacy 2 dataset (Li et al., 2025), which can substantially cover the spatial gaps in the original ACER database. We obtained these data from public sources or directly from the

authors and used them to create an update: ACER2 (Harrison et al., 2025b), which contains 233 additional records covering some part or all of MIS 3 (note that the original ACER records are not included in ACER2 due to licensing issue). The two datasets are combined in our analyses to serve as the fossil pollen dataset (Supplementary Materials, section 3) to reconstruct the past climates. We focus on the 279 records (253 terrestrial records and 26 marine records) between 50 and 30 ka (Figure 1b; Table 1). The fossil pollen data are taxonomically harmonised to be consistent with the SMPDSv3. ~~Here we focus on the 73 records covering most of Marine Isotope Stage 3 (50-30 ka); 54 of these records are from terrestrial sites and 19 from marine sites (Figure 1; Table 1). The fossil data were taxonomically harmonised to be consistent with the SMPDSv3.~~

2.2. Climate reconstruction method

We use~~d~~ *fx*-corrected T~~t~~olerance-weighted Weighted Averaging Partial Least Squares ~~with *fx* correction~~ (*fx*TWA-PLS: Liu et al., 2020, 2023) regression to derive the pollen-climate relationships ~~model the relationships between taxon abundances and individual climate variables~~ in the ~~SMPDSv3~~ modern training dataset, and then apply~~ied~~ these relationships to reconstruct past climates from~~using~~ the fossil ~~assemblages from the ACER database~~pollen records (Figure 2). *fx*TWA-PLS reduces the tendency of regression methods to compress reconstructions towards the centre of the sampled climate range by applying a sampling frequency correction to reduce the influence of uneven sampling of climate space and weighting the contribution of individual taxa according to their climate tolerances (Liu et al., 2020). Version 2 of *fx*TWA-PLS (*fx*TWA-PLSv2: Liu et al., 2023) uses P-splines smoothing to derive the frequency correction and applies this correction both in estimating the climate optima and tolerances, and in the regression itself, producing a further improvement in model performance compared to *fx*TWA-PLSv1 (Liu et al., 2020).

We choose *fx*TWA-PLSv2 here. The evaluation is made by comparing the reconstructions made using modern pollen data with modern climates using leave-out cross-validation~~We evaluated the *fx*TWA-PLSv2 models by comparing the reconstructions with observations using leave-out cross-validation~~, where one site at a time i~~was~~ randomly selected as a test site and sites that are both geographically close (within 50 km horizontal distance from the site) and climatically close (within 2% of the full range of each climate variable in the dataset) a~~we~~re also removed from the training set, to prevent redundancy in the climate information from inflating the cross-validation goodness of fit, following Liu et al. (2020). This ensures that we are not just tuning

to the training dataset, and that we can reconstruct climates even when the training set does not completely cover the climate to be reconstructed because there are gaps in the climate space. Performance is assessed using R^2 and RMSEP (root-mean-square error of prediction), and compression is assessed using linear regression of the leave-out cross-validated reconstructions against the climate variable. The last significant number of components ($p \leq 0.01$) is selected to avoid overfitting due to the increase in the number of components. ~~We selected the last significant number of components (p-value $\leqslant$ 0.01) and assessed model performance using the root mean square error of prediction (RMSEP). Compression was assessed using linear regression of the leave-out cross-validated reconstructions on to the climate variable.~~ Reconstructions of MTCO, MTWA and α_{plant}~~α~~ a~~w~~ere then made for every sample in each fossil record, using the last significant number of components. ~~Sample specific errors were estimated via bootstrapping, as described in Liu et al. (2020).~~ Sample-specific errors are estimated via bootstrapping (resampling the training set 1000 times) as described in Liu et al. (2020).

However, the low CO_2 at glacial period could lead to potential bias between reconstructed and actual plant-available moisture. Atmospheric CO_2 concentration has a direct impact on plant physiological processes, by modulating water-use efficiency (WUE), that is the ratio of carbon uptake to water loss through the stomata (Hatfield and Dold, 2019). The low CO_2 during the glacial period led to reduced water use efficiency (Farquhar, 1997; Gerhart and Ward, 2010; Prentice and Harrison, 2009). Statistical reconstructions cannot take this into account since they are based on modern relationships between pollen assemblages and climate under recent CO_2 levels (Bartlein et al., 2011; Chevalier et al., 2020). The actual conditions under low CO_2 should be wetter than the vegetation-based reconstructions of moisture variables (Prentice et al., 2017, 2022a). (Prentice et al. (, 2022a) provides a way of correction as follows:

$$e(MTGR_1, MI_1, c_{a1}) = e(MTGR_0, MI_0, c_{a0}) \quad (1)$$

where e is the ratio of water loss to CO_2 uptake, a function of the mean temperature of the growing season (MTGR), moisture index (MI) and atmospheric CO_2 concentration (c_a). For MTGR and c_a, the subscript "1" denotes the past value, and the subscript "0" denotes the modern value. MI_0 is the reconstructed uncorrected past value, MI_1 is the "true" past value (to be estimated). The equation means that the "true" MI under past atmospheric conditions should produce the same e with the reconstructed uncorrected MI under modern atmospheric conditions, i.e. those pertaining to the modern pollen calibration dataset.

We transfer our reconstructed past α_{plant} back to the uncorrected moisture index MI_0, and apply the CO_2 correction to obtain the actual moisture index MI_1, then transfer it to actual plant-available moisture $\alpha_{plant,corrected}$ (Figure 2; Figures S2-1 & S2-2). Past and modern values of CO_2 concentrations are taken from ~~(~~Bereiter et al.~~,~~ (2015), following Prentice et al. (2022a). Past MTGR values are inferred by sinusoidal interpolation of reconstructed MTCO and MTWA, assuming that the growing season corresponds to the period with temperatures > 0˚C. Modern MTGR values are obtained using a geographically-weighted regression (GWR) of climatological values (1961-1990) from the Climatic Research Unit Time-Series version 4.04 (CRU TS4.04; Harris et al., 2020) dataset averaged over the period 1961–1990, in order to correct for elevation differences between the CRU grid cells and the fossil pollen sites. The elevations of marine sites are set to 0 when applying GWR.

The CO_2 correction is implemented through the package COdos 0.0.2 (Prentice et al., 2022b) with one modification, as follows. We found when applying the correction in cases where the temperature reduction from modern was large (> 5˚C) that the use of different temperature values to calculate the stomatal sensitivity term (ξ) and the compensation point (Γ*) in the correction algorithm sometimes produced an unrealistically large countervailing effect due to the temperature difference alone. To avoid this problem, we calculate these physiological quantities (ξ and Γ*) using the mean of $MTGR_1$ and $MTGR_0$.~~We corrected for the effect of changes in atmospheric CO_2 on plant water-use efficiency, and hence the reconstructions of α (Figure S2), following Prentice et al. (2022). Appropriate values of CO_2 were taken from the WAIS Divide ice core record (Bauska et al., 2021).~~

2.3. Age modelling of fossil records

~~Although~~ Both the ACER and ACER2 database provide~~s~~ age models for each pollen record.~~,~~ However, the resolutions of the individual records ~~is~~are variable (~~mean resolution 476 years~~ranging from 57 years to 13415 years) and these age models are often imperfectly aligned with the dating of D-O warming events as recorded in the Greenland ice core, and which have been shown to have a globally synchronous imprint through analysis of speleothem records (Adolphi et al., 2018; Corrick et al., 2020). To create a better alignment, we ~~kept the original age model for marine sites since they are generally calibrated using the oxygen isotope records and are therefore more compatible with the ice core records, and~~ use~~d~~ dynamic time warping (DTW: Alshehri et al., 2019; Burstyn et al., 2021; Giorgino, 2009) to adjust the age scale for

each individual terrestrial record (Figure 2). Dynamic time warping optimises the similarity between two sequences (one "query" and one "reference") by stretching or compressing one sequence in the time dimension to match the other. It adjusts the age scale without influencing the variable values, thus retaining the original amplitude of change.

LOVECLIM simulation (Menviel et al., 2014) (covering the interval 50-30 ka) is currently the only published simulation that has attempted to reproduce the specific timing and magnitude of successive D-O cycles. It is coupled ocean-atmosphere-vegetation general circulation model of intermediate complexity. The model was spun up to equilibrium using an initial atmospheric CO_2 concentration of 207.5 ppm, orbital forcing appropriate for 50 ka BP, and an estimate of the 50 ka BP ice-sheet orography and albedo obtained from an off-line ice-sheet model simulation (Abe-Ouchi et al., 2007). After this initialization, the model was forced by time-varying changes in orbital parameters, atmospheric trace gas concentrations and ice-sheet configurations following Timm et al. (2008). In addition, meltwater pulses were added in the North Atlantic in such a way as to reproduce observed sea-surface temperature (SST) variations along the Iberian margin (Martrat et al., 2007). The simulations have proved adequate to capture at least broad features of actual D-O events, and generally consistent with the qualitative signals in Voelker (2002) compilation (Liu et al., 2022). We convert the age scale of LOVECLIM simulations to the Antarctic Ice Core Chronology 2012 (AICC2012) time scale (Veres et al., 2013).

W~~Here, we use simulated mean annual temperature (MAT) from a transient simulation of the interval 50-30 ka made with the LOVECLIM model (Menviel et al., 2014) as the reference sequence to MAT calculated as the average of MTCO and MTWA reconstructed from the individual pollen records. We used the mid-point between the start dates of each D-O warming event as recorded in the Greenland ice core (Wolff et al., 2010; converted into AICC2012 timescale) to sub-divide each ACER record into discrete intervals and modified the time scale of the reconstructed mean annual temperature series in each interval to match the reference sequence, having normalised both sequences to remove the influence of differences in absolute values and the amplitude of changes.~~ e treat the mean annual temperature (MAT) calculated as the average of MTCO and MTWA reconstructed from each individual fossil pollen record as the "query" time series, and find the corresponding grid cell (the location of this fossil pollen record) in LOVECLIM simulations, and use the simulated MAT at this grid cell as the "reference" time series. We further divide each "query" and "reference" time series into

discrete intervals using the mid-points between the start dates of each D-O warming event as recorded in the Greenland ice core (Wolff et al., 2010; converted into AICC2012 timescale), and normalize both time series in each interval to remove the influence of differences in absolute values and the amplitude of changes. Then we apply dynamic time warping to modify the time scale of the "query" to match the "reference" in each interval. The adjusted age model for each ~~ACER~~ fossil record i~~wa~~s then applied to the reconstructions of MTCO, MTWA, ~~and~~ α_{plant} and $\alpha_{plant,corrected}$ from that record for subsequent analyses.

2.4. Assessment of regional climate changes during Greenland D-O warming events

The magnitude of climate change during the interval corresponding to each D-O warming event as registered in Greenland is calculated individually for each climate variable at each site. To avoid making an assumption about the sign of the climate change at a site, we use~~d~~ a third-order polynomial to fit the reconstructions during the interval from 300 years before to 600 years after the official start date corresponding to Greenland D-O warming for each event (Wolff et al., 2010; converted into AICC2012 timescale) to determine whether the change was positive or negative. We then find~~ound~~ the ages where this polynomial curve reaches ~~corresponding to~~ the minimum and maximum ~~in the fitted polynomial~~ ($t_{min,}$ ~~polynomial~~~~,~~ and $t_{max,}$ ~~polynomial~~). Since the smoothed polynomial may underestimate or overestimate the amplitude of change, we use~~d~~ the ~~reconstructed~~ reconstructions ~~minimum or maximum value~~corresponding to $t_{min,polynomial}$ and $t_{max,polynomial}$ to obtain the changes ~~within the period $t_{min\ polynomial}$ ± 100 years or $t_{max\ polynomial}$ ± 100 years respectively~~ (see Figure S3 for illustration). Whether it's an increasing or decreasing signal depends on whether $t_{min,polynomial}$ occurs before or after $t_{max,polynomial}$. The change of each climate variable (ΔV) is calculated as:

~~In cases where no change was registered for all of the three climate variables, we assume that the event was not registered at the site. As a measure of the accuracy of the DTW method to identify D-O events, we compared the number of identified events with the number of D-O events that should occur during the time covered by each record (Table 1). To assess whether events were missed in a particular record due to low sampling resolution, we examined the number of samples present in the 900-year interval covering the sampled D-O (i.e. 300 years before to 600 years after the official start date of each event), where low resolution was defined as ≤ 3 samples in this 900-year interval. Reconstructions covering intervals where a signal was not identified were not used in subsequent analyses.~~

$$\Delta V = V_{end} - V_{start} \quad (2)$$

where V_{start} is the reconstructed value at the start and V_{end} is the reconstructed value at the end of the event. The error of change ($\sigma_{\Delta V}$) is calculated using the following equation assuming V_{start} and V_{end} are independent:

$$\sigma_{\Delta V} = \sqrt{\sigma_{V_{end}}^2 + \sigma_{V_{start}}^2} \quad (3)$$

where σ_{Vstart} is the sample-specific error of V_{start} and σ_{Vend} is the sample-specific error of V_{end}~~We calculated sample-specific errors for the minimum and maximum reconstructed values. Assuming that the minimum and maximum values are independent~~., ~~we used error propagation to obtain the error of the change:~~

To obtain the relationships between changes in different climate variables,

~~Following Liu et al. (2022),~~ we use~~d~~ a maximum likelihood method to estimate the ratio of ΔMTCO to ΔMTWA ~~(~~and the ratio of $\Delta\alpha_{plant,corrected}$~~α~~ to ΔMTWA~~)~~ to take account of the errors on both variables, ~~f.~~ Following Liu et al. (2022).~~,~~

As a measure of the accuracy of the DTW method to identify D-O events, we compare~~d~~ the number of identified events with the number of D-O events that should occur during the time covered by each record (Table 1). To assess whether events a~~w~~ere missed in a particular record due to low sampling resolution, we examine~~d~~ the number of samples present in the 900-year interval covering the sampled D-O (i.e. 300 years before to 600 years after the official start date corresponding to Greenland D-O warming for~~of~~ each event), where low resolution ~~wa~~is defined as ≤ 3 samples in this 900-year interval.

3. Results

*fx*TWA-PLS reproduces the modern climate reasonably well (Table 2; Figure~~s~~ S4~~-~~.1 & 4~~-~~.2). ~~.~~ The performance is best for MTCO (R^2 = 0.74, RMSEP = 6.66, slope = 0.84) but is also good for MTWA (R^2 = 0.60, RMSEP = 3.63, slope = 0.72) and α_{plant} (R^2 = 0.63, RMSEP = 0.186, slope = 0.68)~~The performance is best for MTCO (R^{2-} = 0.75, RMSEP = 6.52, slope = 0.85) but is also good for MTWA (R^{2-} = 0.60, RMSEP = 3.58, slope = 0.72) and α (R^{2-} = 0.65, RMSEP = 0.183, slope = 0.71)~~. Assessment of the variance inflation factor scores shows that there is no

problem of multicollinearity so that it is possible to reconstruct all three climate variables independently (Supplementary Table 1).

The use of dynamic time warping makesde it possible to identify D-O events robustly (Figures S5-1 to~ S5-8; Table 1; Supplementary Table 2). ~~13 of the 73 sites cover some part of the 50-30 ka periods but do not include D-O events.~~ Some sites provide records in 50-30 ka but do not cover the intervals of the D-O events; some marine sites are too far from the land to extract GWR modern MTGR to apply CO_2 correction. Across the remaining 17960 sites which should have D-O events registered, we have identified 544 ~~285~~ out of the 696328 individual ~~D-O~~ events (7887 %) ~~that should occur during the intervals covered by the records~~. In the majority of cases where a D-O event should have been registered but could not be identified in an individual record (13437 out of 15243 cases), the resolution of that part of the record iswas extremely poor ~~(≤ 3 samples in the 900-year interval starting 300 years before to 600 years after the official start date of the event)~~.

~~ΔMTCO and ΔMTWA were generally largest in the extratropics and were more muted in the tropics (Figure 3). ΔMTCO was found to be significantly larger than ΔMTWA in the northern extratropics when considered across all D-O events and sites; ΔMTCO was found to be larger than ΔMTWA, but not significantly larger, in the southern extratropics; ΔMTCO was found to be not correlated with ΔMTWA in the tropics (Table 3). However, there was a significant positive relationship between the Δα and ΔMTWA in all regions (Figure 4; Table 4).~~ ΔMTCO is found to be significantly larger than ΔMTWA in the northern extratropics and tropics when considered across all D-O events and sites, indicating reduced seasonal contrast between winter and summer temperatures; ΔMTCO is found to be larger than ΔMTWA, but not significantly larger, in the southern extratropics (Figure 3; Table 3). There is no globally consistent relationship between $\Delta\alpha_{plant,corrected}$ and ΔMTWA, although the positive relationship in the tropics is marginally significant (Figure 4; Table 4).

The spatial patterns of ΔMTCO and ΔMTWA are generally consistent across multiple D-O events (Figure 5), most noticeably that the largest warming occurs in Eurasia, while western North America and the southern extratropics are characterised by cooling. These patterns are also shown if only reconstructions where the change is twice the error of change are considered (Figure S6), proving that the spatial patterns are robust to the choice of threshold. Nevertheless, both the magnitude of the changes and the spatial patterns vary between the D-O events

(Figures S7-1 & S7-2). Strong events such as D-O 8 show more apparent changes (whether warming or cooling), as well as a strong antiphasing between northern and southern extratropical changes; while weak events such as D-O 9 show less apparent changes with almost no north-south antiphasing (Figure 6).

The changes in plant-available moisture are less spatially coherent that the changes in temperature (Figure 5). There is an increase in $\alpha_{plant,corrected}$ in some regions characterised by warming, for example, southeastern China and Japan; but there are mixed signals of drying and wetting in other regions characterised by warming, such as southern Europe. Furthermore, regions characterised by cooling, such as western North America and southern extratropics, can also show both drying and wetting. Changes in $\Delta\alpha_{plant,corrected}$ also show more variability between D-O events than changes in temperature (Figure S7-4).

~~The spatial patterns of ΔMTCO and ΔMTWA show consistent features across multiple D-O events (Figure 5), most noticeably that the largest warming occurs in the extratropics of Eurasia, while western North America and the southern extratropics are characterised by cooling. These patterns are also shown if only those reconstructions where the change is twice that of the sample specific error are considered (Figure S6), showing that the spatial patterns are robust to the choice of threshold. The anti-phasing between the northern and southern extratropics is consistent across D-O events. Nevertheless, both the magnitude of the changes and the spatial patterns vary between the D-O events (Figure S7.1; Figure S7.2). Δα broadly follows the changes in temperature, with increased α in regions characterised by warming (Figure 5) but show more variability both spatially and between D-O events (Figure S7.3). This is particularly true for Europe, which is characterised by a mixed signal of drying and wetting.~~

4. Discussion and Conclusions

4.1. Comparison with previous reconstructions

We have presented a first attempt to map the spatial patterns of quantitative changes in seasonal temperatures and plant-available moisture during D-O events globally, using a consistent methodology ~~and a single data source~~. These analyses show that there is an anti-phasing

between changes in the northern extratropics and the southern extratropics, with warming in the north and cooling in the south. The largest and most consistent warming during D-O events occurs in Eurasia. There is a significant difference ~~in the~~between winter warming ~~during winter~~ and summer warming in the northern extratropics, resulting in an overall reduction in seasonality~~, but no significant difference in the southern extratropics~~. Site-based reconstructions from the Eifel region in central Europe, based on branched glycerol dialkyl glycerol tetraethers, indicate minimal temperature changes during summer (Zander et al., 2024) and thus support the idea that the D-O changes were driven by large changes in winter temperature. ~~(~~Zumaque et al., (2025) provide seasonal temperature and precipitation reconstructions for 12 of the sites from southern Europe (which are included in our fossil pollen records) but using the modern analogue technique as the reconstruction method and the Eurasian Modern Pollen Database version 2 (Davis et al., 2020) (EMPDv2; also included in our SMPDSv3) as the modern training dataset. They show relatively stable summer temperatures but large change in MTCO through the MIS3 D-O events, consistent with our reconstructions (using a regression-based reconstruction method and a global modern training dataset) of a reduction in seasonality during warming events in the northern extratropics. We find no significant difference in the magnitude of seasonal warming in the southern extratropics. Since only quantitative reconstructions of MAT (rather than MTCO and MTWA) are available from the southern extratropics (e.g. Fletcher and Thomas, 2010; Newnham et al., 2017), there is no independent confirmation of this result.

Qualitative interpretation of palaeo-records suggest that some many regions are characterised by both warming and wetting, such as western Europe (Fletcher et al., 2010; Sánchez-Goñi et al., 2008), eastern Europe (Fleitmann et al., 2009; Stockhecke et al., 2016), central Siberia (Grygar et al., 2006), and the Great Basin USA (Denniston et al., 2007; Jiménez-Moreno et al., 2010). Previous studies have also indicated drier conditions during D-O events, particularly in parts of the USA such as the Pacific Northwest (Grigg and Whitlock, 2002) and Florida (Grimm et al., 2006; Jiménez-Moreno et al., 2010). Our reconstructions show more mixed signals and that there is no globally consistent relationship between changes in temperature and moisture, either in regions characterised by warming or by cooling (Figure 4; Figure 5). We have applied a correction for low CO_2 values during the glacial period to plant-available moisture. The actual values ($\alpha_{plant,corrected}$) are generally higher than the vegetation-based reconstructed values (α_{plant}) (Figure S2-1). However, the correction does not have a significant impact on the spatial patterns during D-O events (Figure S2-2; Figure S7-3).

4.2. Global training dataset vs local training dataset

~~Site-based reconstructions (e.g. Denton et al., 2022; Zander et al., 2024) suggest much larger cooling in winter than summer during cold phases of the last glacial, implying enhanced seasonality compared to warm intervals, which would be consistent with our reconstructions of a reduction in seasonality during warming events in the northern extratropics. Globally, there is a positive relationship between the change in temperature and plant available moisture, as indicated by α. This is consistent with more qualitative interpretation of palaeo-records from specific regions, where many regions, such as western Europe (Fletcher et al., 2010; Sánchez-Goñi et al., 2008), eastern Europe (Fleitmann et al., 2009; Stockhecke et al., 2016), central Siberia (Grygar et al., 2006), and the Great Basin USA (Denniston et al., 2007; Jiménez-Moreno et al., 2010), are characterised by both warming and wetting. However, according to our reconstructions, the nature of this relationship varies between regions: there are some regions that are characterised by warming and wetting, others are characterised by warming and drying (Figure 4; Figure 5). Previous studies have also indicated drier conditions during D-O events, particularly in parts of the USA such as the Pacific Northwest (Grigg and Whitlock, 2002) and Florida (Grimm et al., 2006; Jiménez-Moreno et al., 2010). Although there is some consistency in the broadscale patterns of changes across D-O events, the magnitude of the changes as well as the spatial patterning varies between events (Figure S7.1~ 7.3).~~

We have used a global pollen ~~data set~~dataset for calibration of the pollen-climate relationships. In general, reconstructions of glacial climates have used region-specific data sets (e.g. Dugerdil et al., 2021, 2025; Newnham et al., 2017; Wei et al., 2021; Zumaque et al., 2025). ~~(~~Herzschuh et al.~~,~~ (2023) made this explicit in their reconstructions of northern hemisphere climate over the past 30,000 years, by restricting the modern training data to within a 2000 km radius of individual fossil sites. The use of a region-specific raining data set can be justified on the grounds that it produces better statistics for the modern-day relationship between pollen abundance and specific climate variables. Nevertheless, as pointed out by ~~(~~Chevalier et al. (~~,~~ 2020), an important issue is that the modern calibration data set has a span that adequately samples the climate space experienced in the past. The use of a global dataset for calibration makes it possible to sample a larger range of climates, and specifically to reconstruct climates that might be very different from the modern range in that region. For example, reconstructions of past European climate (Figure S8) based on region-specific training dataset would yield less extreme winter temperatures than reconstructed using the global training data set. Although the

trend and spatial pattern might not be influenced greatly, the amplitude of change might be underestimated.

The use of a global ~~data set~~dataset, rather than region-specific training data, relies on the principle of phylogenetic niche conservatism (Harvey and Pagel, 1991; Qian and Ricklefs, 2004; Wang et al., 2025), which states that traits tend to remain constant over time. This also applies to the climate niche (Crisp and Cook, 2012; Jiang et al., 2023; Peterson, 2011; Wiens et al., 2010; Wiens and Graham, 2005) as evidenced by disjunct distributions of taxa across different continents (Yin et al., 2021). Niche conservatism underpins the fact that the modern distribution of specific genera can be predicted using climate-pollen relationships developed from other regions (e.g. Huntley et al., 1989). ~~The use of a global dataset for calibration makes it possible to sample a large range of climates, and specifically to reconstruct climate variables that might be very different from the range experienced in a region in the modern day. This is particularly important when reconstructing changes in the fundamentally different climate of the last glacial. Reconstructed glacial climates at some sites were indeed found to exceed the climate ranges sampled for the region under modern conditions, most noticeably MTCO and MTWA in the southern extratropics (Figure S8).~~ However, the use of a global ~~data set~~dataset can create issues because of inconsistencies in taxonomic resolution between regions. The necessity for treating all species of *Quercus* as a single taxon, despite the fact that evergreen and deciduous species may occupy distinct climate niches in some regions ~~such as Europe~~, is a consequence of this. However, we have shown (Supplementary Materials, s~~S~~ection 4) that this has little impact on our reconstructions – largely because the climatic distinction that would be conveyed through separating deciduous and evergreen *Quercus* is also registered by the presence of other taxa. Although the use of a global training ~~data set~~dataset for climate reconstructions has not been a common practice, it addresses the need to ensure that the modern training data adequately represents past climate conditions and also facilitates making reconstructions for sites from regions with limited modern pollen data. ~~it also facilitates making reconstructions for sites from regions with limited modern pollen data or where the modern samples do not capture the very different climates that might have occurred in that region during glacial times.~~

4.3. Targets for model evaluation

The~~se~~ reconstructions in this paper can be used as targets for model evaluation, specifically the two transient D-O experiments planned for the next phase of the Palaeoclimate Modelling

Intercomparison (see Malmierca-Vallet et al., 2023 for the experimental protocol). The first of these experiments is a baseline simulation starting at 34 ka, a time with low obliquity, moderate MIS3 greenhouse gas values, and an intermediate ice sheet configuration, which appears to be most conducive to generating D-O like behaviour in climate models. The second experiment involves the addition of freshwater, to examine whether this is necessary to precondition a state conducive to generating D-O events. The ~~observed~~ anti-phasing in reconstructed temperature changes between the northern and southern hemispheres is a general feature of climate model experiments. Most models show larger warming in winter than in summer in the northern hemisphere (e.g. Flückiger et al., 2008; Izumi et al., 2023; Van Meerbeeck et al., 2011), which is also consistent with our reconstructions. However, the cooling in western North America during D-O warming events in our reconstructions is not a feature of all climate model simulations.

Models generally show an intensification of the northern hemisphere monsoons during D-O events (e.g. Izumi et al., 2023; Menviel et al., 2020), but there is less consistency about changes in plant-available moisture in the extratropics. Our reconstructions show an increase in $\alpha_{plant,corrected}$ in southeastern China and Japan (Figure 5)~~Our reconstructions of α suggest an intensification of the northern hemisphere monsoons. , consistent with the simulations, and provide an opportunity to evaluate spatial patterns of moisture changes over the extratropics. The reconstructions also indicate an increase in α across much of the tropics, including northern South America, southern China and Japan (Figure 5).~~ Although $\alpha_{plant,corrected}$~~α~~ is not a direct reflection of summer precipitation, these changes are consistent with enhanced northern hemisphere monsoons during D-O warming events, as shown by speleothem records from the Caribbean (Warken et al., 2019) and speleothem and pollen records from Asia (Fohlmeister et al., 2023; Wang et al., 2001; Zorzi et al., 2022). However, there are more spatial variability and mixed signals.

The LOVECLIM model wa~~i~~s used as a reference to adjust the age scale in the reconstructions using MAT, but this does not preclude comparison of the ~~reconstructed and simulated~~ seasonal temperatures. Here we approximate the winter-season temperature as MTCO and summer-season temperature as MTWA, since monthly temperatures are not available (only seasonal temperatures are available) in LOVECLIM. -The general spatial pattern of simulated changes in MTCO and MTWA (Figure ~~S9.1~~7) is consistent with the reconstructions, with largest warming in Eurasia, and cooling ~~over most of the~~ in the southern extratropic~~sal land~~. The

simulated changes are strong during D-O 8 but weak during D-O 9 (Figures 9-1 & 9-2), again as shown by the reconstructions. However, there are important differences. For example, simulated changes generally have smaller amplitude than shown by the reconstructions, and the cooling over western North America is generally only in winter, while t~~T~~he reconstructions show cooling over ~~western North America~~this region in both seasons~~, for example, but only in winter in the simulations~~. The relationship between ΔMTCO ~~versus~~ and ΔMTWA is also different (Figure ~~S9.2~~8; Table 5): the simulated ΔMTCO is shown to be significantly larger than ΔMTWA in the northern extratropics, but significantly smaller than ΔMTWA in the southern extratropics, a contrast that is not so marked in the reconstructions. ~~the simulated ΔMTCO is shown to be significantly larger than ΔMTWA in the northern extratropics, but significantly smaller than ΔMTWA in the southern extratropics (Supplementary Table 3).~~ This comparison illustrates the usefulness of the reconstructions for model evaluation and to investigate the mechanisms that may not be adequately captured by current models.

4.4. Others

Identifying D-O events in pollen records is often problematic, particularly in regions where warming (especially if accompanied by dryer conditions) leads to a reduction (or an hiatus) in sedimentation as reflected in the variable resolution of the available pollen records (e.g. Camuera et al., 2022; Pini et al., 2022; Sinopoli et al., 2019; Wei et al., 2021). The use of dynamic time warping ~~(Alshehri et al., 2019; Burstyn et al., 2021; Giorgino, 2009)~~ goes some way to improving the identification of potential D-O events. However, it precludes the calculation of a rate of change in climate. Thus, we have focused here on the ~~absolute~~ magnitude of the changes during specific warming events. It is also likely that some of the variability in the reconstructed changes between different D-O events reflects imperfect identification of specific events because of the comparatively modest resolution of the records. ~~Several new high-resolution records covering MIS3 have become available since the compilation of the ACER database (e.g. Bird et al., 2024; Camuera et al., 2022; Pini et al., 2022; Rowe et al., 2024; Shichi et al., 2023; Wei et al., 2021; Zorzi et al., 2022) and including these newer records could help to improve the reliability of the global reconstructions presented here.~~

Data and code availability. All the data used are public access and cited here. The code used to generate the reconstructions and figures is available at https://github.com/ml4418/DO-climate-reconstruction-paper.git (will upload to zenodo in the final version).

Author contributions. ML, SPH and ICP designed the study. ML made the reconstructions and produced the figures and tables. ML and SPH carried out the analyses. SPH wrote the first draft of the paper and all authors contributed to the final draft.

Competing Interests. The authors declare not competing interests.

Acknowledgements. ~~ML~~ ML acknowledges support from Imperial College through the Lee Family Scholarship. ICP acknowledges support from the ERC under the European Union Horizon 2020 research and innovation programme (grant agreement no.: 787203 REALM). SPH acknowledges fruitful discussions with colleagues from the D-O community working group. We would like to acknowledge our colleagues who provided original pollen data for inclusion in the ACER2 data set: Jon Camuera, Penelope González-Sampériz, Gonzalo Jiménez-Moreno, Xinghi Liu, Rewi Newnham, Jian Ni, Roberta Pini, Cassie Rowe, Frank Sirocco and María Del Socorro Lozano-García.~~acknowledges support from Imperial College through the Lee Family Scholarship. ICP acknowledges support from the ERC under the European Union Horizon 2020 research and innovation programme (grant agreement no.: 787203 REALM). SPH acknowledges fruitful discussions with colleagues from the D-O community working group.~~

References

Abe-Ouchi, A., Segawa, T. and Saito, F.: Climatic conditions for modelling the Northern Hemisphere ice sheets throughout the ice age cycle, Clim. Past, 3(3), 423–438, doi:10.5194/cp-3-423-2007, 2007.

Adolphi, F., Bronk Ramsey, C., Erhardt, T., Edwards, R. L., Cheng, H., Turney, C. S. M., Cooper, A., Svensson, A., Rasmussen, S. O., Fischer, H. and Muscheler, R.: Connecting the Greenland ice-core and U/Th timescales via cosmogenic radionuclides: testing the synchroneity of Dansgaard–Oeschger events, Clim. Past, 14(11), 1755–1781, doi:10.5194/cp-14-1755-2018, 2018.

Alshehri, M., Coenen, F. and Dures, K.: Effective sub-sequence-based dynamic time warping, in Artificial Intelligence XXXVI. SGAI 2019. Lecture Notes in Computer Science, edited by M. Bramer and M. Petridis, p. 11927, Springer, Cham., 2019.

Ampel, L., Bigler, C., Wohlfarth, B., Risberg, J., Lotter, A. F. and Veres, D.: Modest summer temperature variability during DO cycles in western Europe, Quat. Sci. Rev., 29(11), 1322–1327, doi:10.1016/j.quascirev.2010.03.002, 2010.

Bartlein, P. J., Harrison, S. P., Brewer, S., Connor, S., Davis, B. A. S., Gajewski, K., Guiot, J., Harrison-Prentice, T. I., Henderson, A., Peyron, O., Prentice, I. C., Scholze, M., Seppä, H., Shuman, B., Sugita, S., Thompson, R. S., Viau, A. E., Williams, J. and Wu, H.: Pollen-based continental climate reconstructions at 6 and 21 ka: A global synthesis, Clim. Dyn., 37(3), 775–802, doi:10.1007/s00382-010-0904-1, 2011.

Bereiter, B., Eggleston, S., Schmitt, J., Nehrbass-Ahles, C., Stocker, T. F., Fischer, H., Kipfstuhl, S. and Chappellaz, J.: Revision of the EPICA Dome C CO2 record from 800 to 600 kyr before present, Geophys. Res. Lett., 42(2), 542–549, doi:10.1002/2014GL061957, 2015.

Boucher-Lalonde, V., Morin, A. and Currie, D. J.: How are tree species distributed in climatic space? A simple and general pattern, Glob. Ecol. Biogeogr., 21(12), 1157–1166, doi:10.1111/j.1466-8238.2012.00764.x, 2012.

Burstyn, Y., Gazit, A. and Dvir, O.: Hierarchical dynamic time warping methodology for aggregating multiple geological time series, Comput. Geosci., 150, 104704,

645 doi:10.1016/j.cageo.2021.104704, 2021.

646 Camuera, J., Ramos-Román, M. J., Jiménez-Moreno, G., García-Alix, A., Ilvonen, L., Ruha,
647 L., Gil-Romera, G., González-Sampériz, P. and Seppä, H.: Past 200 kyr hydroclimate
648 variability in the western Mediterranean and its connection to the African Humid Periods,
649 Sci. Rep., 12(1), 9050, doi:10.1038/s41598-022-12047-1, 2022.

650 Cao, X., Tian, F., Andreev, A. A., Anderson, P. M., Lozhkin, A. V, Bezrukova, E. V, Ni, J.,
651 Rudaya, N., Stobbe, A., Wieczorek, M. and Herzschuh, U.: A taxonomically harmonized and
652 temporally standardized fossil pollen dataset from Siberia covering the last 40 ka [dataset
653 publication series], PANGAEA, doi:10.1594/PANGAEA.898616, 2019.

654 Cao, X., Tian, F., Andreev, A., Anderson, P. M., Lozhkin, A. V, Bezrukova, E., Ni, J.,
655 Rudaya, N., Stobbe, A., Wieczorek, M. and Herzschuh, U.: A taxonomically harmonized and
656 temporally standardized fossil pollen dataset from Siberia covering the last 40 kyr, Earth
657 Syst. Sci. Data, 12(1), 119–135, doi:10.5194/essd-12-119-2020, 2020.

658 Chevalier, M., Davis, B. A. S., Heiri, O., Seppä, H., Chase, B. M., Gajewski, K., Lacourse,
659 T., Telford, R. J., Finsinger, W., Guiot, J., Kühl, N., Maezumi, S. Y., Tipton, J. R., Carter, V.
660 A., Brussel, T., Phelps, L. N., Dawson, A., Zanon, M., Vallé, F., Nolan, C., Mauri, A., de
661 Vernal, A., Izumi, K., Holmström, L., Marsicek, J., Goring, S., Sommer, P. S., Chaput, M.
662 and Kupriyanov, D.: Pollen-based climate reconstruction techniques for late Quaternary
663 studies, Earth-Science Rev., 210, 103384, doi:10.1016/j.earscirev.2020.103384, 2020.

664 Corrick, E. C., Drysdale, R. N., Hellstrom, J. C., Capron, E., Rasmussen, S. O., Zhang, X.,
665 Fleitmann, D., Couchoud, I. and Wolff, E.: Synchronous timing of abrupt climate changes
666 during the last glacial period, Science (80-.)., 369(6506), 963 LP – 969,
667 doi:10.1126/science.aay5538, 2020.

668 Crisp, M. D. and Cook, L. G.: Phylogenetic niche conservatism: What are the underlying
669 evolutionary and ecological causes?, New Phytol., 196(3), 681–694, doi:10.1111/j.1469-
670 8137.2012.04298.x, 2012.

671 Dansgaard, W., Johnsen, S. J., Clausen, H. B., Dahl-Jensen, D., Gundestrup, N. S., Hammer,
672 C. U., Hvidberg, C. S., Steffensen, J. P., Sveinbjörnsdottir, A. E., Jouzel, J. and Bond, G.:
673 Evidence for general instability of past climate from a 250-kyr ice-core record, Nature,

364(6434), 218–220, doi:10.1038/364218a0, 1993.

Davis, B. A. S., Chevalier, M., Sommer, P., Carter, V. A., Finsinger, W., Mauri, A., Phelps, L. N., Zanon, M., Abegglen, R., Åkesson, C. M., Alba-Sánchez, F., Anderson, R. S., Antipina, T. G., Atanassova, J. R., Beer, R., Belyanina, N. I., Blyakharchuk, T. A., Borisova, O. K., Bozilova, E., Bukreeva, G., Bunting, M. J., Clò, E., Colombaroli, D., Combourieu-Nebout, N., Desprat, S., Di Rita, F., Djamali, M., Edwards, K. J., Fall, P. L., Feurdean, A., Fletcher, W., Florenzano, A., Furlanetto, G., Gaceur, E., Galimov, A. T., Gałka, M., Garc\'\ia-Moreiras, I., Giesecke, T., Grindean, R., Guido, M. A., Gvozdeva, I. G., Herzschuh, U., Hjelle, K. L., Ivanov, S., Jahns, S., Jankovska, V., Jiménez-Moreno, G., Karpińska-Kołaczek, M., Kitaba, I., Kołaczek, P., Lapteva, E. G., Latałowa, M., Lebreton, V., Leroy, S., Leydet, M., Lopatina, D. A., López-Sáez, J. A., Lotter, A. F., Magri, D., Marinova, E., Matthias, I., Mavridou, A., Mercuri, A. M., Mesa-Fernández, J. M., Mikishin, Y. A., Milecka, K., Montanari, C., Morales-Molino, C., Mrotzek, A., Muñoz Sobrino, C., Naidina, O. D., Nakagawa, T., Nielsen, A. B., Novenko, E. Y., Panajiotidis, S., Panova, N. K., Papadopoulou, M., Pardoe, H. S., Pędziszewska, A., Petrenko, T. I., Ramos-Román, M. J., Ravazzi, C., Rösch, M., Ryabogina, N., Sabariego Ruiz, S., Salonen, J. S., Sapelko, T. V, Schofield, J. E., Seppä, H., Shumilovskikh, L., Stivrins, N., Stojakowits, P., Svobodova Svitavska, H., Święta-Musznicka, J., Tantau, I., Tinner, W., Tobolski, K., Tonkov, S., Tsakiridou, M., et al.: The Eurasian Modern Pollen Database (EMPD), Version 2, Earth Syst. Sci. Data Discuss., 2020, 1–41, doi:10.5194/essd-2020-14, 2020.

Davis, T. W., Prentice, I. C., Stocker, B. D., Thomas, R. T., Whitley, R. J., Wang, H., Evans, B. J., Gallego-Sala, A. V, Sykes, M. T. and Cramer, W.: Simple process-led algorithms for simulating habitats (SPLASH v.1.0): Robust indices of radiation, evapotranspiration and plant-available moisture, Geosci. Model Dev., 10(2), 689–708, doi:10.5194/gmd-10-689-2017, 2017.

Denniston, R. F., Asmerom, Y., Polyak, V., Dorale, J. A., Carpenter, S. J., Trodick, C., Hoye, B. and González, L. A.: Synchronous millennial-scale climatic changes in the Great Basin and the North Atlantic during the last interglacial, Geology, 35(7), 619–622, doi:10.1130/G23445A.1, 2007.

Dima, M., Lohmann, G. and Knorr, G.: North Atlantic versus global control on Dansgaard-Oeschger events, Geophys. Res. Lett., 45(23), 12,912-991,998, doi:10.1029/2018GL080035,

2018.

Doblas-Reyes, F. J., Sörensson, A. A., Almazroui, M., Dosio, A., Gutowski, W. J., Haarsma, R., Hamdi, R., Hewitson, B., Kwon, W.-T., Lamptey, B. L., Maraun, D., Stephenson, T. S., Takayabu, I., Terray, L., Turner, A. and Zuo, Z.: Linking global to regional climate change, in Climate Change 2021 – The Physical Science Basis: Working Group I Contribution to the Sixth Assessment Report of the Intergovernmental Panel on Climate Change, edited by V. Masson-Delmotte, P.Zhai, A. Pirani, S. L. Connors, C. Péan, S. Berger, N. Caud, Y. Chen, L. Goldfarb, M. I. Gomis, M. Huang, K. Leitzell, E.Lonnoy, J. B. R. Matthews, T. K. Maycock, T. Waterfield, O. Yelekçi, R. Yu, and B. Zhou, pp. 1363–1512, Cambridge University Press, Cambridge, United Kingdom and New York, NY, USA., 2021.

Dugerdil, L., Joannin, S., Peyron, O., Jouffroy-Bapicot, I., Vannière, B., Boldgiv, B., Unkelbach, J., Behling, H. and Ménot, G.: Climate reconstructions based on GDGT and pollen surface datasets from Mongolia and Baikal area: calibrations and applicability to extremely cold–dry environments over the Late Holocene, Clim. Past, 17(3), 1199–1226, doi:10.5194/cp-17-1199-2021, 2021.

Dugerdil, L., Peyron, O., Ménot, G., Egamberdieva, D., Alimov, J., Leroy, S. A. G., Garnier, E., Nowak, A. and Joannin, S.: First paleoenvironmental calibrations for modern pollen rain of Tajikistan and Uzbekistan: A case study of pollen - vegetation functional biogeography of Arid Central Asia, Glob. Planet. Change, 252, 104857, doi:10.1016/j.gloplacha.2025.104857, 2025.

Farquhar, G. D.: Carbon dioxide and vegetation, Science (80-.)., 278(5342), 1411, doi:10.1126/science.278.5342.1411, 1997.

Fleitmann, D., Cheng, H., Badertscher, S., Edwards, R. L., Mudelsee, M., Göktürk, O. M., Fankhauser, A., Pickering, R., Raible, C. C., Matter, A., Kramers, J. and Tüysüz, O.: Timing and climatic impact of Greenland interstadials recorded in stalagmites from northern Turkey, Geophys. Res. Lett., 36(19), doi:10.1029/2009GL040050, 2009.

Fletcher, M.-S. and Thomas, I.: A quantitative Late Quaternary temperature reconstruction from western Tasmania, Australia, Quat. Sci. Rev., 29(17), 2351–2361, doi:10.1016/j.quascirev.2010.06.012, 2010.

734 Fletcher, W. J., Sánchez-Goñi, M. F., Allen, J. R. M., Cheddadi, R., Combourieu-Nebout, N.,
735 Huntley, B., Lawson, I., Londeix, L., Magri, D., Margari, V., Müller, U. C., Naughton, F.,
736 Novenko, E., Roucoux, K. and Tzedakis, P. C.: Millennial-scale variability during the last
737 glacial in vegetation records from Europe, Quat. Sci. Rev., 29(21), 2839–2864,
738 doi:10.1016/j.quascirev.2009.11.015, 2010.

739 Flückiger, J., Knutti, R., White, J. W. C. and Renssen, H.: Modeled seasonality of glacial
740 abrupt climate events, Clim. Dyn., 31(6), 633–645, doi:10.1007/s00382-008-0373-y, 2008.

741 Fohlmeister, J., Sekhon, N., Columbu, A., Vettoretti, G., Weitzel, N., Rehfeld, K., Veiga-
742 Pires, C., Ben-Yami, M., Marwan, N. and Boers, N.: Global reorganization of atmospheric
743 circulation during Dansgaard–Oeschger cycles, Proc. Natl. Acad. Sci., 120(36),
744 e2302283120, doi:10.1073/pnas.2302283120, 2023.

745 Gerhart, L. M. and Ward, J. K.: Plant responses to low [CO_2] of the past, New Phytol.,
746 188(3), 674–695, doi:10.1111/j.1469-8137.2010.03441.x, 2010.

747 Giorgino, T.: Computing and visualizing Dynamic Time Warping alignments in R: The dtw
748 package, J. Stat. Softw., 31(7 SE-Articles), 1–24, doi:10.18637/jss.v031.i07, 2009.

749 Grigg, L. D. and Whitlock, C.: Patterns and causes of millennial-scale climate change in the
750 Pacific Northwest during Marine Isotope Stages 2 and 3, Quat. Sci. Rev., 21(18), 2067–2083,
751 doi:10.1016/S0277-3791(02)00017-3, 2002.

752 Grimm, E. C., Watts, W. A., Jacobson, G. L., Hansen, B. C. S., Almquist, H. R. and
753 Dieffenbacher-Krall, A. C.: Evidence for warm wet Heinrich events in Florida, Quat. Sci.
754 Rev., 25(17), 2197–2211, doi:10.1016/j.quascirev.2006.04.008, 2006.

755 Grygar, T., Kadlec, J., Pruner, P., Swann, G., Bezdička, P., Hradil, D., Lang, K., Novotna, K.
756 and Oberhänsli, H.: Paleoenvironmental record in Lake Baikal sediments: Environmental
757 changes in the last 160 ky, Palaeogeogr. Palaeoclimatol. Palaeoecol., 237(2), 240–254,
758 doi:10.1016/j.palaeo.2005.12.007, 2006.

759 Guiot, J., de Beaulieu, J. L., Cheddadi, R., David, F., Ponel, P. and Reille, M.: The climate in
760 Western Europe during the last Glacial/Interglacial cycle derived from pollen and insect
761 remains, Palaeogeogr. Palaeoclimatol. Palaeoecol., 103(1), 73–93, doi:10.1016/0031-
762 0182(93)90053-L, 1993.

763 Harris, I., Osborn, T. J., Jones, P. and Lister, D.: Version 4 of the CRU TS monthly high-
764 resolution gridded multivariate climate dataset, Sci. Data, 7, 109, doi:10.1038/s41597-020-
765 0453-3, 2020.

766 Harrison, S., Egbudom, M.-A. and Villegas-Diaz, R.: The SPECIAL Modern Pollen Data Set
767 for Climate Reconstructions, version 3 (SMPDSv3), , doi:10.17864/1947.001473, 2025a.

768 Harrison, S. P.: Climate reconstructions for the SMPDS v1 modern pollen data set, Univ.
769 Read., doi:10.5281/zenodo.3605003, 2020.

770 Harrison, S. P. and Sanchez-Goñi, M. F.: Global patterns of vegetation response to
771 millennial-scale variability and rapid climate change during the last glacial period, Quat. Sci.
772 Rev., 29(21), 2957–2980, doi:10.1016/j.quascirev.2010.07.016, 2010.

773 Harrison, S. P., Egbudom, M.-A. and Liu, M.: ACER2: The Abrupt Climate Changes and
774 Environmental Responses Database (version 2), , doi:10.17864/1947.001449, 2025b.

775 Harrison, S. P., Bartlein, P. J., Cruz-Silva, E., Haas, O., Jackson, S. T., Kaushal, N., Liu, M.,
776 Magri, D., Robson, D., Vettoretti, G. and Prentice, I. C.: Palaeoclimate perspectives on
777 contemporary climate change, Ann. Rev. Environ. Resour., 50, 2025c.

778 Harvey, P. H. and Pagel, M. D.: The comparative method in evolutionary biology, Oxford
779 University Press., 1991.

780 Hatfield, J. L. and Dold, C.: Water-use efficiency: Advances and challenges in a changing
781 climate, Front. Plant Sci., Volume 10, doi:10.3389/fpls.2019.00103, 2019.

782 Herzschuh, U., Böhmer, T., Li, C., Chevalier, M., Hébert, R., Dallmeyer, A., Cao, X.,
783 Bigelow, N. H., Nazarova, L., Novenko, E. Y., Park, J., Peyron, O., Rudaya, N. A., Schlütz,
784 F., Shumilovskikh, L. S., Tarasov, P. E., Wang, Y., Wen, R., Xu, Q. and Zheng, Z.:
785 LegacyClimate 1.0: a dataset of pollen-based climate reconstructions from 2594 Northern
786 Hemisphere sites covering the last 30 kyr and beyond, Earth Syst. Sci. Data, 15(6), 2235–
787 2258, doi:10.5194/essd-15-2235-2023, 2023.

788 Huber, C., Leuenberger, M., Spahni, R., Flückiger, J., Schwander, J., Stocker, T. F., Johnsen,
789 S., Landais, A. and Jouzel, J.: Isotope calibrated Greenland temperature record over Marine
790 Isotope Stage 3 and its relation to CH_4, Earth Planet. Sci. Lett., 243(3), 504–519,

791 doi:10.1016/j.epsl.2006.01.002, 2006.

792 Huntley, B., Bartlein, P. J. and Prentice, I. C.: Climatic control of the distribution and
793 abundance of Beech (Fagus L.) in Europe and North America, J. Biogeogr., 16(6), 551–560,
794 doi:10.2307/2845210, 1989.

795 Huntley, B., Watts, W. A., Allen, J. R. M. and Zolitschka, B.: Palaeoclimate, chronology and
796 vegetation history of the Weichselian Lateglacial: comparative analysis of data from three
797 cores at Lago Grande di Monticchio, southern Italy, Quat. Sci. Rev., 18(7), 945–960,
798 doi:10.1016/S0277-3791(99)00007-4, 1999.

799 IPCC: Climate change 2022: Impacts, adaptation and vulnerability. Contribution of working
800 group II to the sixth assessment report of the Intergovernmental Panel on Climate Change,
801 edited by H.-O. Pörtner, D. C. Roberts, M. Tignor, E. S. Poloczanska, K. Mintenbeck, A.
802 Alegría, M. Craig, S. Langsdorf, S. Löschke, V. Möller, A. Okem, and B. Rama, Cambridge
803 University Press, Cambridge University Press, Cambridge, UK and New York, NY, USA.,
804 2022.

805 Izumi, K., Armstrong, E. and Valdes, P.: Global footprints of dansgaard-oeschger oscillations
806 in a GCM, Quat. Sci. Rev., 305, 108016, doi:10.1016/j.quascirev.2023.108016, 2023.

807 Jiang, K., Wang, Q., Dimitrov, D., Luo, A., Xu, X., Su, X., Liu, Y., Li, Y., Li, Y. and Wang,
808 Z.: Evolutionary history and global angiosperm species richness–climate relationships, Glob.
809 Ecol. Biogeogr., 32(7), 1059–1072, doi:10.1111/geb.13687, 2023.

810 Jiménez-Moreno, G., Anderson, R. S., Desprat, S., Grigg, L. D., Grimm, E. C., Heusser, L.
811 E., Jacobs, B. F., López-Martínez, C., Whitlock, C. L. and Willard, D. A.: Millennial-scale
812 variability during the last glacial in vegetation records from North America, Quat. Sci. Rev.,
813 29(21), 2865–2881, doi:10.1016/j.quascirev.2009.12.013, 2010.

814 Kindler, P., Guillevic, M., Baumgartner, M., Schwander, J., Landais, A. and Leuenberger,
815 M.: Temperature reconstruction from 10 to 120 kyr b2k from the NGRIP ice core, Clim. Past,
816 10(2), 887–902, doi:10.5194/cp-10-887-2014, 2014.

817 Lapellegerie, P., Millet, L., Rius, D., Duprat-Oualid, F., Luoto, T. and Heiri, O.: Chironomid-
818 inferred summer temperature during the Last Glacial Maximum in the Southern Black Forest,
819 Central Europe, Quat. Sci. Rev., 345, 109016, doi:10.1016/j.quascirev.2024.109016, 2024.

Lee, J.-Y., Marotzke, J., Bala, G., Cao, L., Corti, S., Dunne, J. P., Engelbrecht, F., Fischer, E., Fyfe, J. C., Jones, C., Maycock, A., Mutemi, J., Ndiaye, O., Panickal, S. and Zhou, T.: Future global climate: Scenario-based projections and near-term information, in Climate change 2021: The physical science basis. Contribution of working group I to the sixth assessment report of the Intergovernmental Panel on Climate Change, edited by V. Masson-Delmotte, P. Zhai, A. Pirani, S. L. Connors, C. Péan, S. Berger, N. Caud, Y. Chen, L. Goldfarb, M. I. Gomis, M. Huang, K. Leitzell, E. Lonnoy, J. B. R. Matthews, T. K. Maycock, T. Waterfield, O. Yelekçi, R. Yu, and B. Zhou, pp. 553–672, Cambridge University Press, Cambridge, United Kingdom and New York, NY, USA., 2021.

Li, C., Ni, J., Böhmer, T., Cao, X., Zhou, B., Liao, M., Li, K., Schild, L., Wieczorek, M., Heim, B. and Herzschuh, U.: LegacyPollen2.0: an updated global taxonomically and temporally standardized fossil pollen dataset of 3680 palynological records, , doi:10.1594/PANGAEA.965907, 2025.

Liu, M., Prentice, I. C., ter Braak, C. J. F. and Harrison, S. P.: An improved statistical approach for reconstructing past climates from biotic assemblages, Proc. R. Soc. A Math., 476(2243), 20200346, doi:10.1098/rspa.2020.0346, 2020.

Liu, M., Prentice, I. C., Menviel, L. and Harrison, S. P.: Past rapid warmings as a constraint on greenhouse-gas climate feedbacks, Commun. Earth Environ., 3, 196, doi:10.1038/s43247-022-00536-0, 2022.

Liu, M., Shen, Y., González-Sampériz, P., Gil-Romera, G., ter Braak, C. J. F., Prentice, I. C. and Harrison, S. P.: Holocene climates of the Iberian Peninsula: pollen-based reconstructions of changes in the west–east gradient of temperature and moisture, Clim. Past, 19(4), 803–834, doi:10.5194/cp-19-803-2023, 2023.

Malmierca-Vallet, I., Sime, L. C. and Members, the D. community: Dansgaard–Oeschger events in climate models: Review and baseline Marine Isotope Stage 3 (MIS3) protocol, Clim. Past, 19(5), 915–942, doi:10.5194/cp-19-915-2023, 2023.

Martrat, B., Grimalt, J. O., Shackleton, N. J., de Abreu, L., Hutterli, M. A. and Stocker, T. F.: Four climate cycles of recurring deep and surface water destabilizations on the Iberian margin, Science (80-.)., 317(5837), 502–507, doi:10.1126/science.1139994, 2007.

Van Meerbeeck, C. J., Renssen, H., Roche, D. M., Wohlfarth, B., Bohncke, S. J. P., Bos, J. A. A., Engels, S., Helmens, K. F., Sánchez-Goñi, M. F., Svensson, A. and Vandenberghe, J.: The nature of MIS 3 stadial–interstadial transitions in Europe: New insights from model–data comparisons, Quat. Sci. Rev., 30(25), 3618–3637, doi:10.1016/j.quascirev.2011.08.002, 2011.

Menviel, L., Timmermann, A., Friedrich, T. and England, M. H.: Hindcasting the continuum of Dansgaard–Oeschger variability: Mechanisms, patterns and timing, Clim. Past, 10(1), 63–77, doi:10.5194/cp-10-63-2014, 2014.

Menviel, L., Skinner, L. C., Tarasov, L. and Tzedakis, P. C.: An ice–climate oscillatory framework for Dansgaard–Oeschger cycles, Nat. Rev. Earth Environ., 1(12), 677–693, doi:10.1038/s43017-020-00106-y, 2020.

Newnham, R. M., Alloway, B. V, Holt, K. A., Butler, K., Rees, A. B. H., Wilmshurst, J. M., Dunbar, G. and Hajdas, I.: Last Glacial pollen–climate reconstructions from Northland, New Zealand, J. Quat. Sci., 32(6), 685–703, doi:10.1002/jqs.2955, 2017.

Peterson, A. T.: Ecological niche conservatism: A time-structured review of evidence, J. Biogeogr., 38(5), 817–827, doi:10.1111/j.1365-2699.2010.02456.x, 2011.

Pini, R., Furlanetto, G., Vallé, F., Badino, F., Wick, L., Anselmetti, F. S., Bertuletti, P., Fusi, N., Morlock, M. A., Delmonte, B., Harrison, S. P., Maggi, V. and Ravazzi, C.: Linking North Atlantic and Alpine Last Glacial Maximum climates via a high-resolution pollen-based subarctic forest steppe record, Quat. Sci. Rev., 294, 107759, doi:10.1016/j.quascirev.2022.107759, 2022.

Prentice, I. C. and Harrison, S. P.: Ecosystem effects of CO_2 concentration: evidence from past climates, Clim. Past, 5(3), 297–307, doi:10.5194/cp-5-297-2009, 2009.

Prentice, I. C., Cleator, S. F., Huang, Y. H., Harrison, S. P. and Roulstone, I.: Reconstructing ice-age palaeoclimates: Quantifying low-CO_2 effects on plants, Glob. Planet. Change, 149, 166–176, doi:10.1016/j.gloplacha.2016.12.012, 2017.

Prentice, I. C., Villegas-Diaz, R. and Harrison, S. P.: Accounting for atmospheric carbon dioxide variations in pollen-based reconstruction of past hydroclimates, Glob. Planet. Change, 211, 103790, doi:10.1016/j.gloplacha.2022.103790, 2022a.

878 Prentice, I. C., Villegas-Diaz, R. and Harrison, S. P.: COdos: CO2 correction tools, ,
879 doi:10.5281/zenodo.5083309, 2022b.

880 Prud'homme, C., Fischer, P., Jöris, O., Gromov, S., Vinnepand, M., Hatté, C., Vonhof, H.,
881 Moine, O., Vött, A. and Fitzsimmons, K. E.: Millennial-timescale quantitative estimates of
882 climate dynamics in central Europe from earthworm calcite granules in loess deposits,
883 Commun. Earth Environ., 3(1), 267, doi:10.1038/s43247-022-00595-3, 2022.

884 Qian, H. and Ricklefs, R. E.: Geographical distribution and ecological conservatism of
885 disjunct genera of vascular plants in eastern Asia and eastern North America, J. Ecol., 92(2),
886 253–265, doi:10.1111/j.0022-0477.2004.00868.x, 2004.

887 Sánchez-Goñi, M., Cacho, I., Turon, J., Guiot, J., Sierro, F., Peypouquet, J., Grimalt, J. and
888 Shackleton, N.: Synchroneity between marine and terrestrial responses to millennial scale
889 climatic variability during the last glacial period in the Mediterranean region, Clim. Dyn.,
890 19(1), 95–105, doi:10.1007/s00382-001-0212-x, 2002.

891 Sánchez-Goñi, M. F., Landais, A., Fletcher, W. J., Naughton, F., Desprat, S. and Duprat, J.:
892 Contrasting impacts of Dansgaard–Oeschger events over a western European latitudinal
893 transect modulated by orbital parameters, Quat. Sci. Rev., 27(11), 1136–1151,
894 doi:10.1016/j.quascirev.2008.03.003, 2008.

895 Sánchez-Goñi, M. F., Desprat, S., Daniau, A.-L., Bassinot, F. C., Polanco-Martínez, J. M.,
896 Harrison, S. P., Allen, J. R. M., Anderson, R. S., Behling, H., Bonnefille, R., Burjachs, F.,
897 Carrión, J. S., Cheddadi, R., Clark, J. S., Combourieu-Nebout, N., Mustaphi, J. C., Debusk,
898 G. H., Dupont, L. M., Finch, J. M., Fletcher, W. J., Giardini, M., González, C., Gosling, W.
899 D., Grigg, L. D., Grimm, E. C., Hayashi, R., Helmens, K., Heusser, L. E., Hill, T., Hope, G.,
900 Huntley, B., Igarashi, Y., Irino, T., Jacobs, B., Jiménez-Moreno, G., Kawai, S., Kershaw, A.
901 P., Kumon, F., Lawson, I. T., Ledru, M.-P., Lézine, A.-M., Liew, P. M., Magri, D., Marchant,
902 R., Margari, V., Mayle, F. E., McKenzie, G. M., Moss, P., Müller, S., Müller, U. C.,
903 Naughton, F., Newnham, R. M., Oba, T., Pérez-Obiol, R., Pini, R., Ravazzi, C., Roucoux, K.
904 H., Rucina, S. M., Scott, L., Takahara, H., Tzedakis, P. C., Urrego, D. H., van Geel, B.,
905 Valencia, B. G., Vandergoes, M. J., Vincens, A., Whitlock, C. L., Willard, D. A. and
906 Yamamoto, M.: The ACER pollen and charcoal database: a global resource to document
907 vegetation and fire response to abrupt climate changes during the last glacial period, Earth
908 Syst. Sci. Data, 9(2), 679–695, doi:10.5194/essd-9-679-2017, 2017.

909 Sinopoli, G., Peyron, O., Masi, A., Holtvoeth, J., Francke, A., Wagner, B. and Sadori, L.:
910 Pollen-based temperature and precipitation changes in the Ohrid Basin (western Balkans)
911 between 160 and 70 ka, Clim. Past, 15(1), 53–71, doi:10.5194/cp-15-53-2019, 2019.

912 Stockhecke, M., Timmermann, A., Kipfer, R., Haug, G. H., Kwiecien, O., Friedrich, T.,
913 Menviel, L., Litt, T., Pickarski, N. and Anselmetti, F. S.: Millennial to orbital-scale variations
914 of drought intensity in the Eastern Mediterranean, Quat. Sci. Rev., 133, 77–95,
915 doi:10.1016/j.quascirev.2015.12.016, 2016.

916 Timm, O., Timmermann, A., Abe-Ouchi, A., Saito, F. and Segawa, T.: On the definition of
917 seasons in paleoclimate simulations with orbital forcing, Paleoceanography, 23(2),
918 doi:10.1029/2007PA001461, 2008.

919 Turner, M. G., Wei, D., Prentice, I. C. and Harrison, S. P.: The impact of methodological
920 decisions on climate reconstructions using WA-PLS, Quat. Res., 99, 341–356,
921 doi:10.1017/qua.2020.44, 2020.

922 Újvári, G., Bernasconi, S. M., Stevens, T., Kele, S., Páll-Gergely, B., Surányi, G. and
923 Demény, A.: Stadial-interstadial temperature and aridity variations in east central Europe
924 preceding the Last Glacial Maximum, Paleoceanogr. Paleoclimatology, 36(8),
925 e2020PA004170, doi:10.1029/2020PA004170, 2021.

926 Veres, D., Bazin, L., Landais, A., Toyé Mahamadou Kele, H., Lemieux-Dudon, B., Parrenin,
927 F., Martinerie, P., Blayo, E., Blunier, T., Capron, E., Chappellaz, J., Rasmussen, S. O.,
928 Severi, M., Svensson, A., Vinther, B. and Wolff, E. W.: The Antarctic ice core chronology
929 (AICC2012): An optimized multi-parameter and multi-site dating approach for the last 120
930 thousand years, Clim. Past, 9(4), 1733–1748, doi:10.5194/cp-9-1733-2013, 2013.

931 Vettoretti, G. and Peltier, W. R.: Interhemispheric air temperature phase relationships in the
932 nonlinear Dansgaard-Oeschger oscillation, Geophys. Res. Lett., 42(4), 1180–1189,
933 doi:10.1002/2014GL062898, 2015.

934 Voelker, A. H. L.: Global distribution of centennial-scale records for Marine Isotope Stage
935 (MIS) 3: a database, Quat. Sci. Rev., 21(10), 1185–1212, doi:10.1016/S0277-3791(01)00139-
936 1, 2002.

937 Wang, C., Wang, M., Zhu, S., Wu, X., Yang, S., Yan, Y. and Wen, Y.: Multiple ecological

938 niche modeling reveals niche conservatism and divergence in East Asian Yew (Taxus),
939 Plants, 14(7), doi:10.3390/plants14071094, 2025.

940 Wang, H., Prentice, I. C. and Ni, J.: Data-based modelling and environmental sensitivity of
941 vegetation in China, Biogeosciences, 10(9), 5817–5830, doi:10.5194/bg-10-5817-2013, 2013.

942 Wang, Y. J., Cheng, H., Edwards, R. L., An, Z. S., Wu, J. Y., Shen, C.-C. and Dorale, J. A.:
943 A high-resolution absolute-dated Late Pleistocene monsoon record from Hulu Cave, China,
944 Science (80-.)., 294(5550), 2345–2348, doi:10.1126/science.1064618, 2001.

945 Warken, S. F., Scholz, D., Spötl, C., Jochum, K. P., Pajón, J. M., Bahr, A. and Mangini, A.:
946 Caribbean hydroclimate and vegetation history across the last glacial period, Quat. Sci. Rev.,
947 218, 75–90, doi:10.1016/j.quascirev.2019.06.019, 2019.

948 Wei, D., Prentice, I. C. and Harrison, S. P.: The climatic space of European pollen taxa,
949 Ecology, 101(8), e03055, doi:10.1002/ecy.3055, 2020.

950 Wei, D., González-Sampériz, P., Gil-Romera, G., Harrison, S. P. and Prentice, I. C.: Seasonal
951 temperature and moisture changes in interior semi-arid Spain from the last interglacial to the
952 Late Holocene, Quat. Res., 101, 143–155, doi:10.1017/qua.2020.108, 2021.

953 Wiens, J. and Graham, C.: Niche conservatism: Integrating evolution, ecology, and
954 conservation biology, Annu. Rev. Ecol. Evol. Syst., 36, 519–539,
955 doi:10.1146/annurev.ecolsys.36.102803.095431, 2005.

956 Wiens, J., Ackerly, D., Allen, A., Anacker, B., Buckley, L., Cornell, H., Damschen, E.,
957 Davies, J., Grytnes, J. A., Harrison, S., Hawkins, B., Holt, R., Mccain, C. and Stephens, P.:
958 Niche conservatism as an emerging principle in ecology and conservation biology, Ecol.
959 Lett., 13, 1310–1324, doi:10.1111/j.1461-0248.2010.01515.x, 2010.

960 Wolff, E. W., Chappellaz, J., Blunier, T., Rasmussen, S. O. and Svensson, A.: Millennial-
961 scale variability during the last glacial: The ice core record, Quat. Sci. Rev., 29(21), 2828–
962 2838, doi:10.1016/j.quascirev.2009.10.013, 2010.

963 Woodward, F. I.: Climate and Plant Distribution, Cambridge University Press, Cambridge,
964 UK., 1987.

965 Yin, X., Jarvie, S., Guo, W.-Y., Deng, T., Mao, L., Zhang, M., Chu, C., Qian, H., Svenning,

J.-C. and He, F.: Niche overlap and divergence times support niche conservatism in eastern Asia–eastern North America disjunct plants, Glob. Ecol. Biogeogr., 30(10), 1990–2003, doi:10.1111/geb.13360, 2021.

Zander, P. D., Böhl, D., Sirocko, F., Auderset, A., Haug, G. H. and Martínez-García, A.: Reconstruction of warm-season temperatures in central Europe during the past 60 000 years from lacustrine branched glycerol dialkyl glycerol tetraethers (brGDGTs), Clim. Past, 20(4), 841–864, doi:10.5194/cp-20-841-2024, 2024.

Zhou, B.-R., Liao, M.-N., Li, K., Xu, D.-Y., Chen, H.-Y., Ni, J., Cao, X.-Y., Kong, Z.-C., Xu, Q.-H., Zhang, Y., Herzschuh, U., Cai, Y.-L., Chen, B.-S., Chen, J.-A., Chen, L.-K., Cheng, B., Gao, Y., Huang, X.-Z., Li, S.-F., Li, W.-Y., Liu, K.-B., Liu, G.-X., Liu, P.-M., Liu, X.-Q., Ma, C.-M., Song, C.-Q., Sun, X.-J., Tang, L.-Y., Wang, M.-H., Wang, Y.-B., Xu, J.-S., Yan, S., Yang, X.-D., Yao, Y.-F., Ye, C.-Y., Zhang, Z.-Y., Zhao, Z.-Y., Zheng, Z. and Zhu, C.: A fossil pollen dataset of China, Chinese J. Plant Ecol., 47(10), 1453–1463 [online] Available from: https://www.plant-ecology.com, 2023.

Zorzi, C., Desprat, S., Clément, C., Thirumalai, K., Oliviera, D., Anupama, K., Prasad, S. and Martinez, P.: When eastern India oscillated between desert versus savannah-dominated vegetation, Geophys. Res. Lett., 49(16), e2022GL099417, doi:10.1029/2022GL099417, 2022.

Zumaque, J., de Vernal, A., Fréchette, B., Guiot, J., Sánchez-Goñi, M. F., Barhoumi, C., Peyron, O., Peros, M., Burke, A., Camuera, J., Jiménez-Moreno, G. and Ramos-Román, M. J.: Decoupled winter and summer climate changes in southern Europe during the Dansgaard-Oeschger cycles, Quat. Sci. Rev., 359, 109273, doi:10.1016/j.quascirev.2025.109273, 2025.

Figures and Tables

Figure 1: Map showing the locations of (a) modern pollen recordssites in version 3 of the SPECIAL Modern Pollen Dataset (SMPDSv3) used to derive the pollen-climate transfer functions for the climate reconstructions, , and (b) fossil pollen recordssites from the Abrupt Climate Changes and Environmental Responses (ACER) database covering the interval between 50- ka and 30 ka used used for the climate reconstructions.

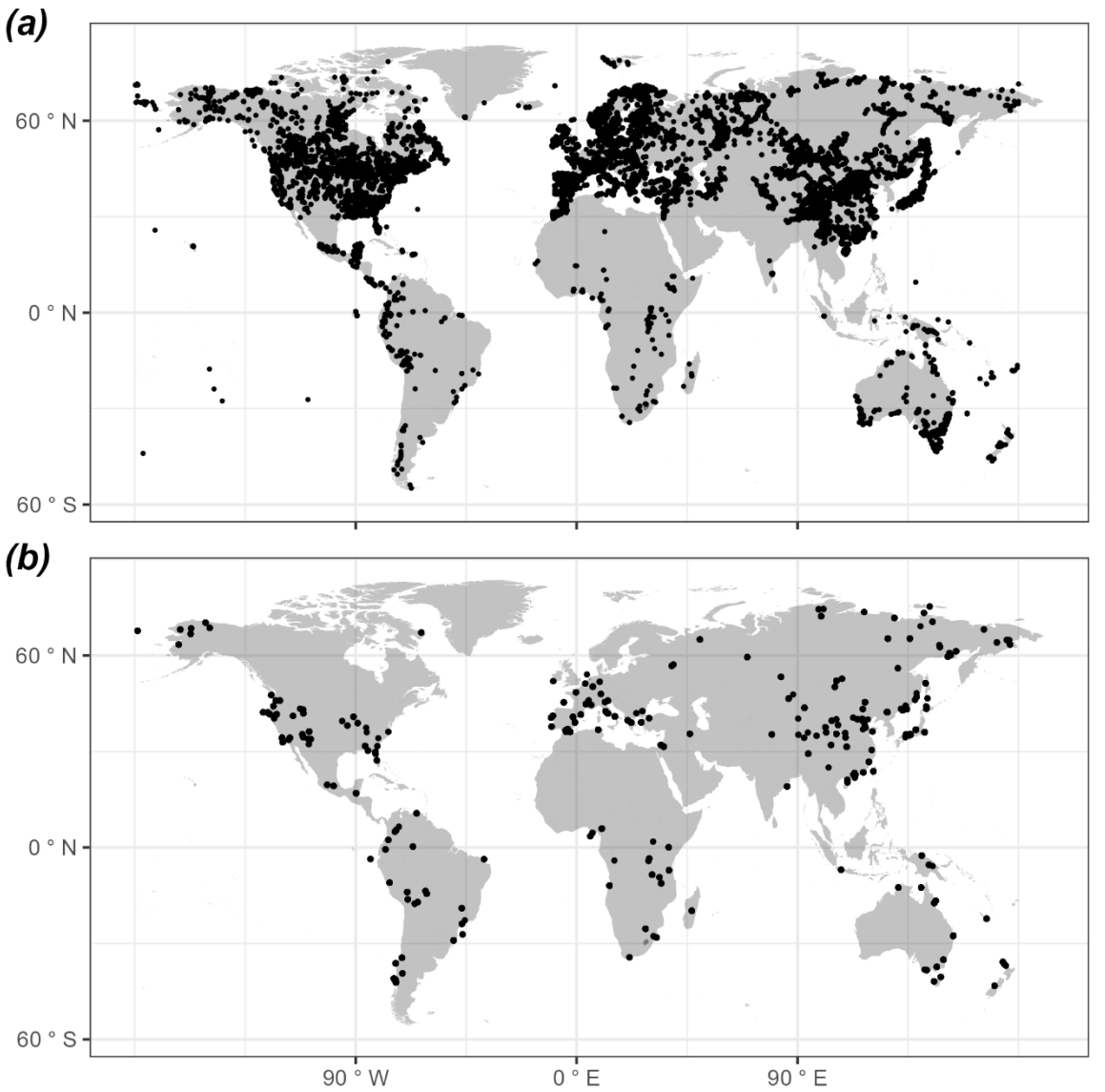

995

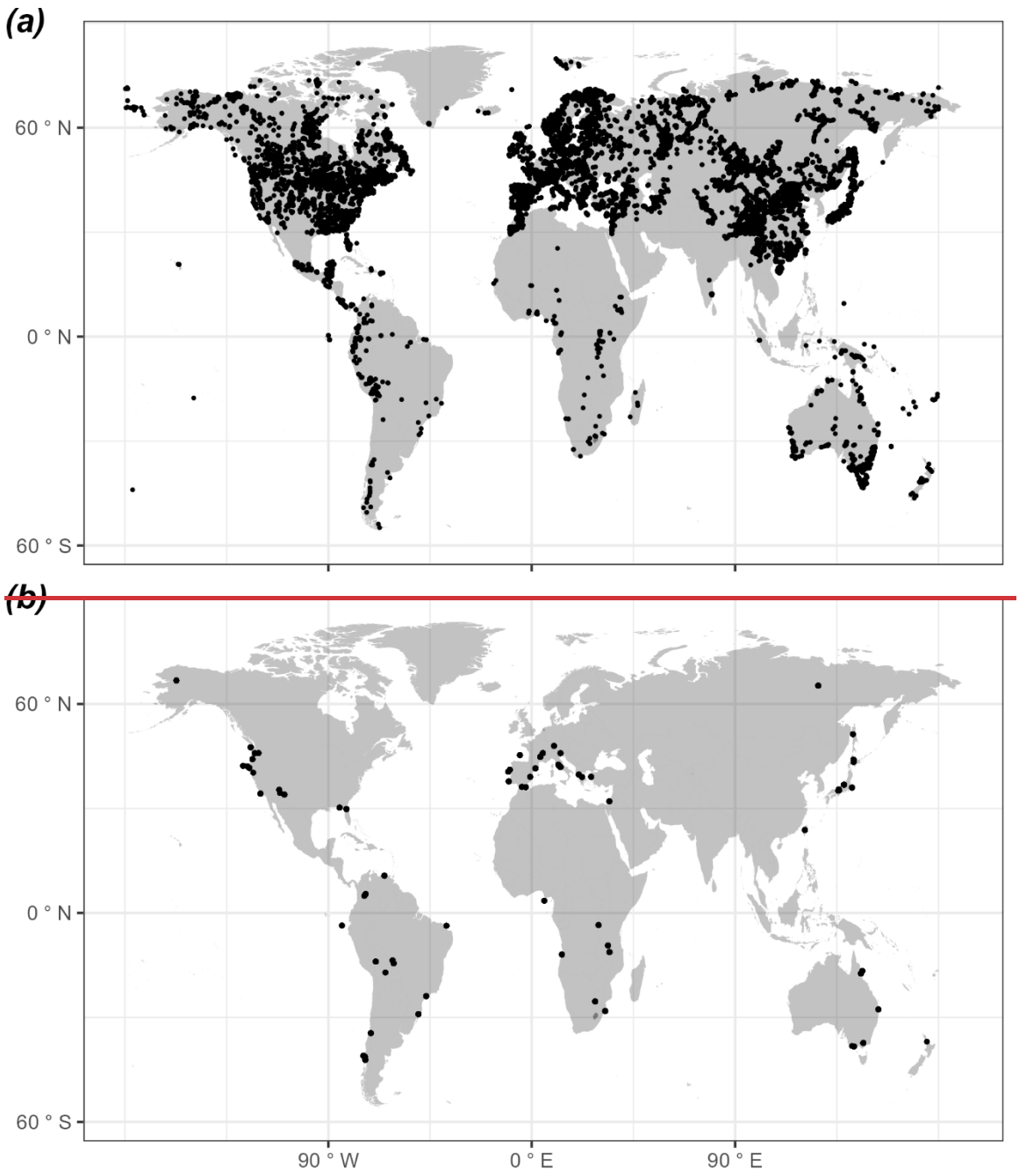

996

997

Figure 2: Flow chart showing the ~~reconstruction~~ methodology.

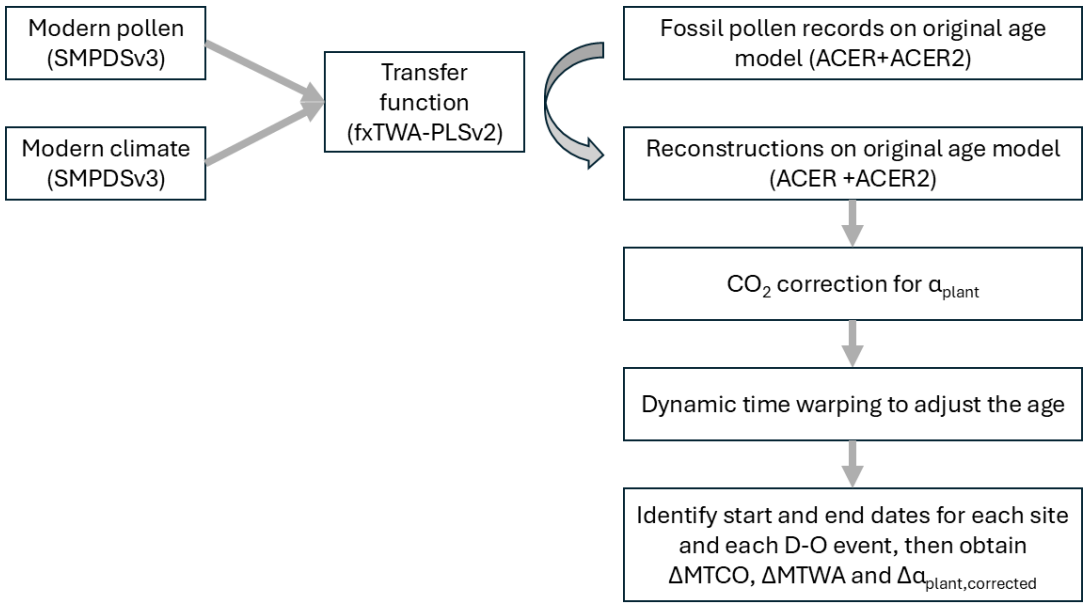

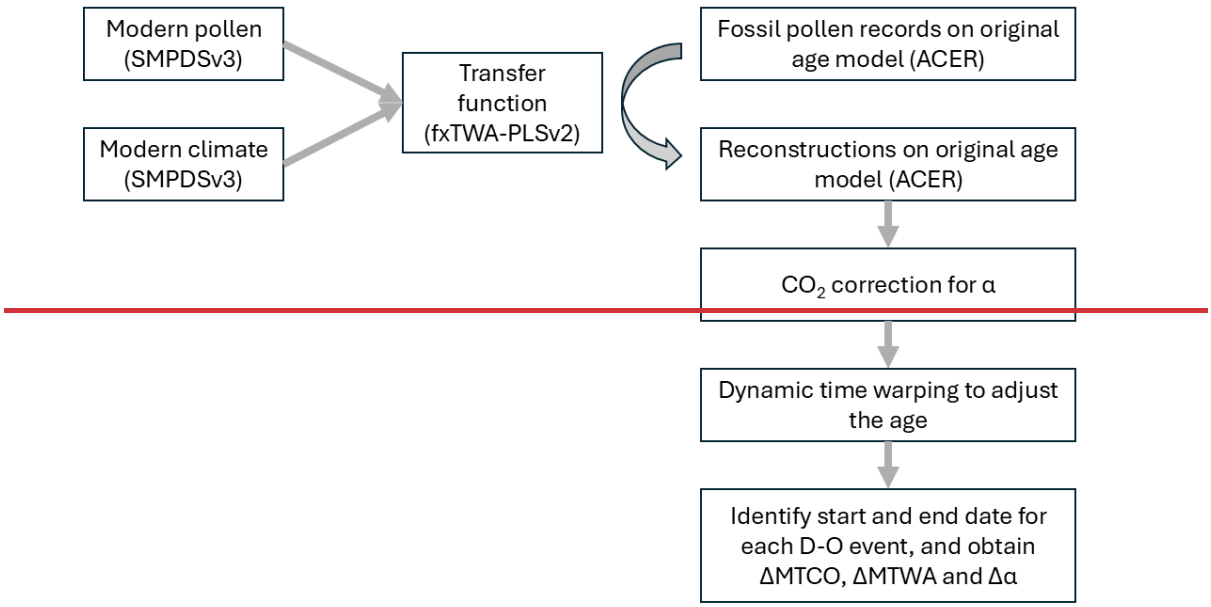

Figure 3: Scatter plot of the change in mean temperature of the coldest month (ΔMTCO) versus the change in mean temperature of the warmest month (ΔMTWA) during individual Dansgaard-Oeschger (D-O) events at individual sites. The points are grouped into~~points are colour-coded to indicate whether the sites are from~~ the northern extratropics (NET, north of 23.5°N), the tropics (TROP, between 23.5°N and 23.5°S) ~~or~~ and the southern extratropics (SET, south of 23.5°S). The grey lines indicate ± 1 error of the change.

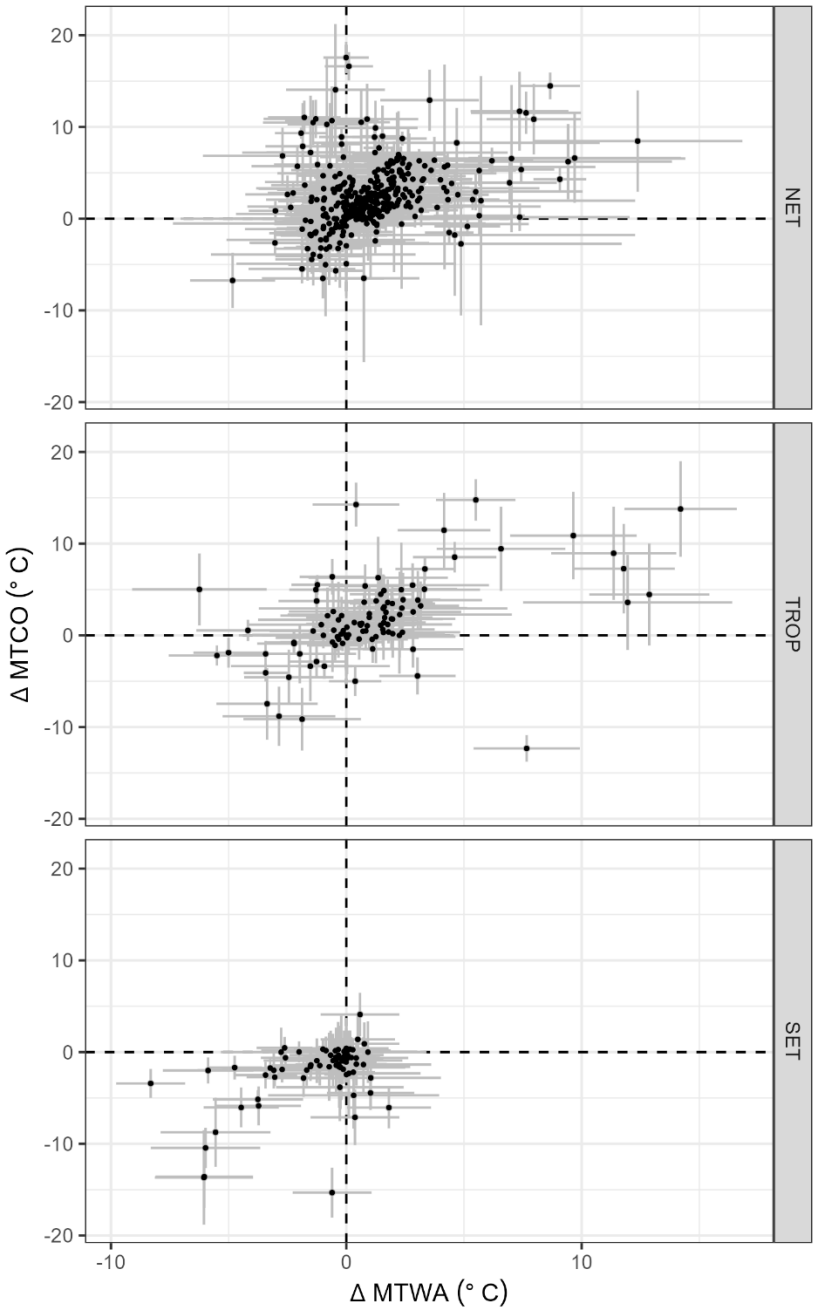

1010

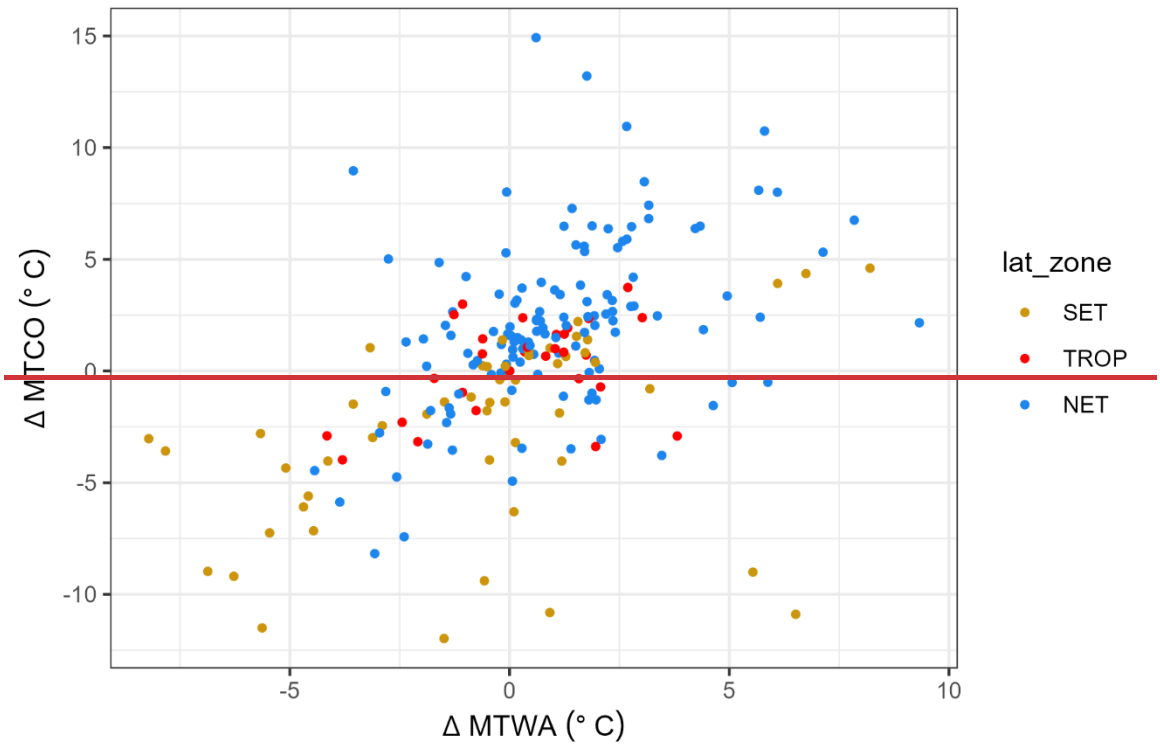

1011

1012

Figure 4: Scatter plot of the change in CO_2-corrected plant-available moisture ($\Delta\alpha_{plant,corrected}$~~$\alpha$~~) versus the change in mean temperature of the warmest month (ΔMTWA) during individual Dansgaard-Oeschger (D-O) events at individual sites. The points are grouped into~~The points are colour-coded to indicate whether the sites are from~~ the northern extratropics (NET, north of 23.5°N), the tropics (TROP, between 23.5°N and 23.5°S) and the~~or~~ southern extratropics (SET, south of 23.5°S). The grey lines indicate ± 1 error of the change.

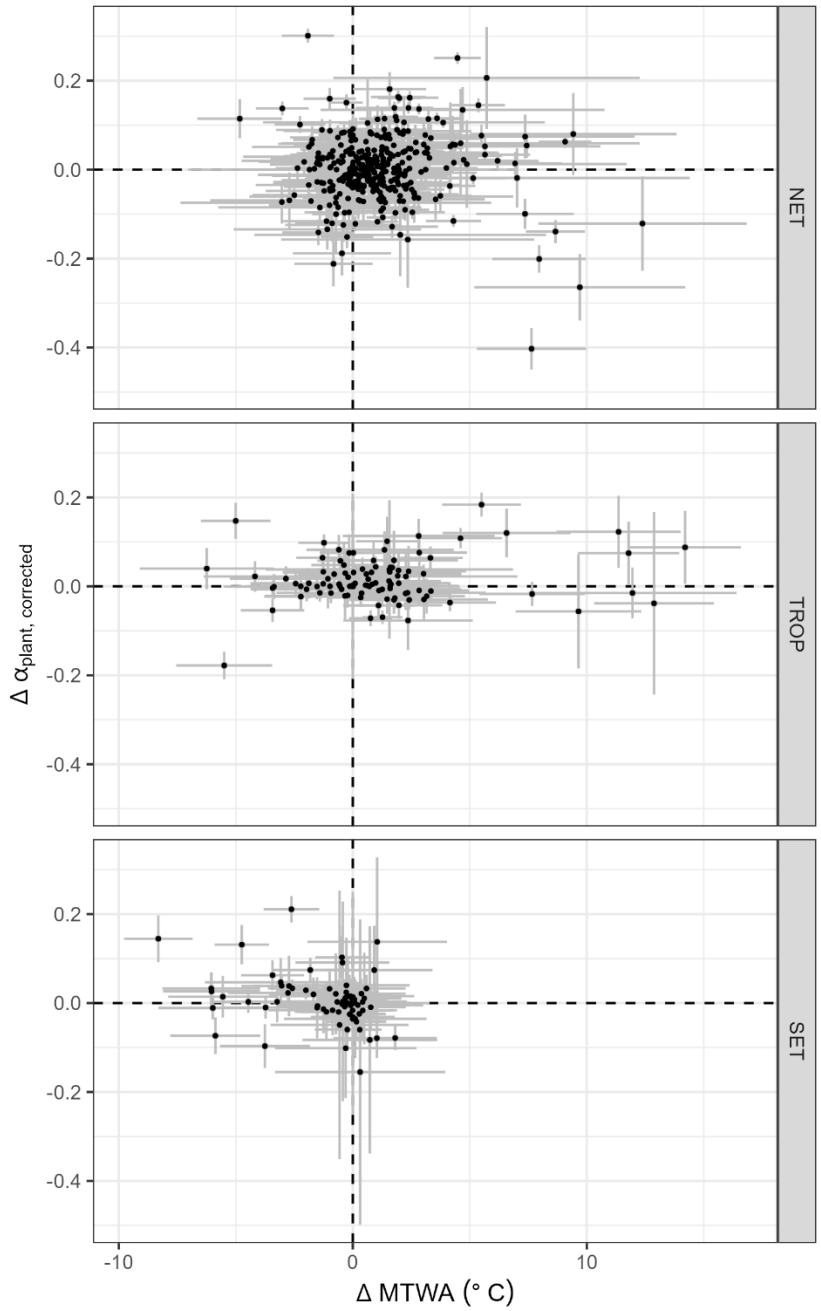

1019

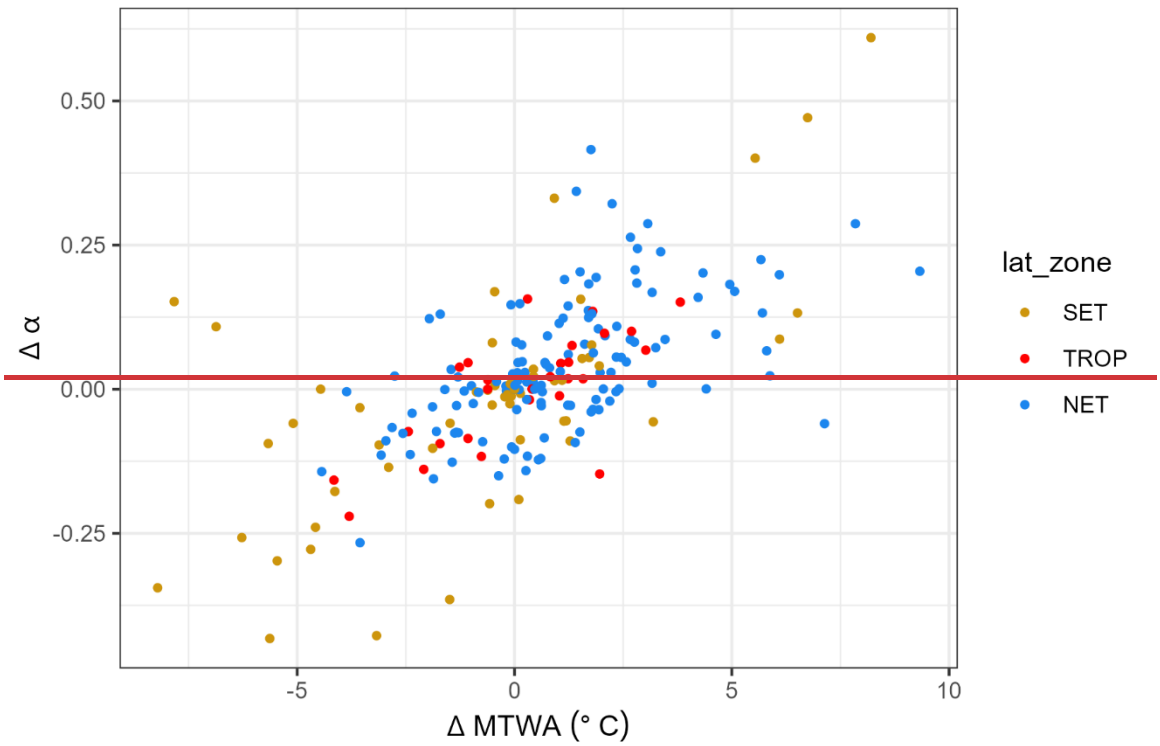

1020

1021

1022 Figure 5: Map~~s~~ showing the median change of site-based reconstructions for Dansgaard-
1023 Oeschger (D-O) events 5 to ~~-~~12. The panels from top to bottom show the changes in mean
1024 temperature of the coldest month (ΔMTCO), mean temperature of the warmest month
1025 (ΔMTWA) and CO_2-corrected plant-available moisture ($\Delta\alpha_{plant,corrected}$).

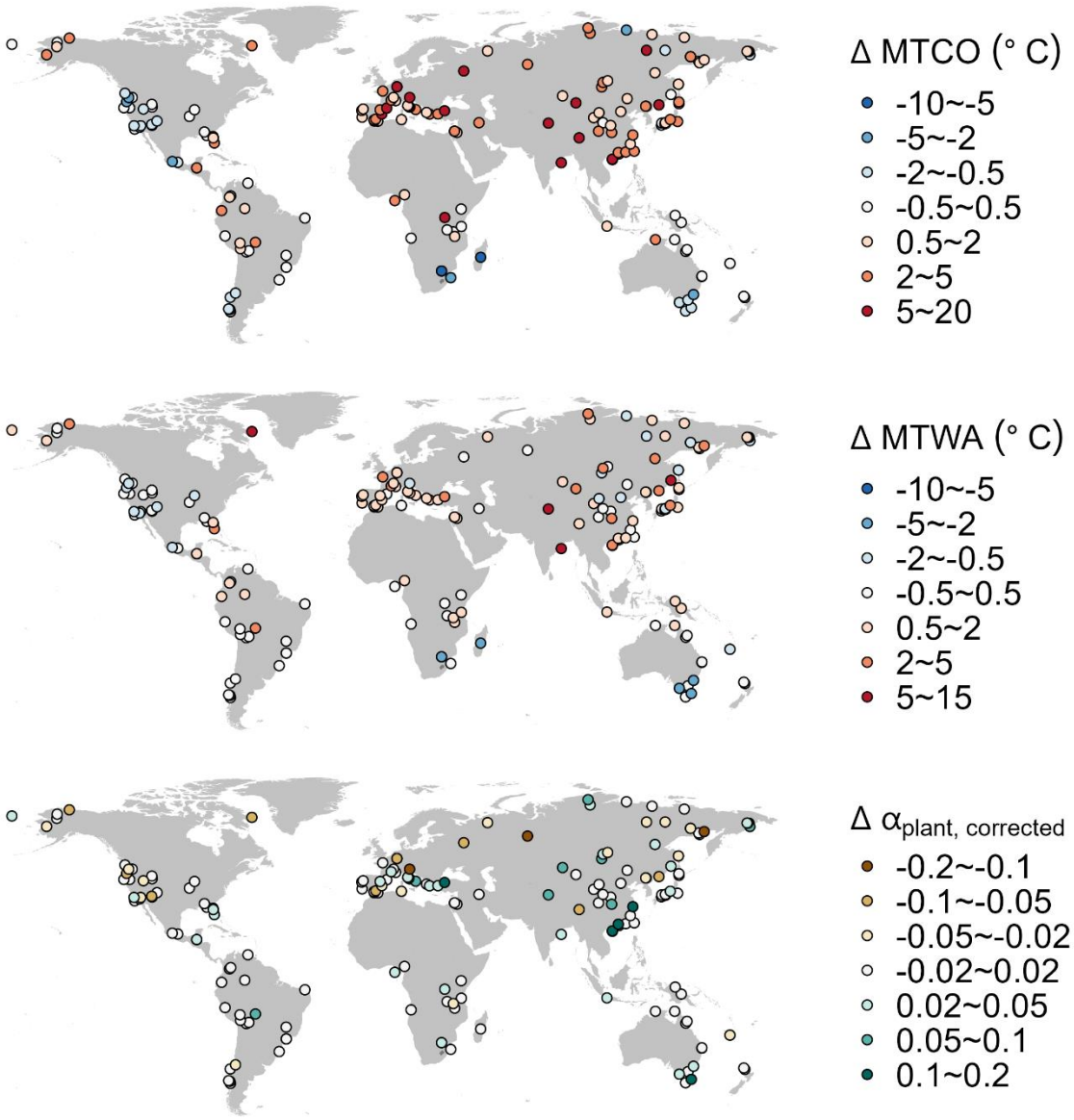
Δ MTCO (° C)
-10~-5
-5~-2
-2~-0.5
-0.5~0.5
0.5~2
2~5
5~20
Δ MTWA (° C)
-10~-5
-5~-2
-2~-0.5
-0.5~0.5
0.5~2
2~5
5~15
Δ αplant, corrected
-0.2~-0.1
-0.1~-0.05
-0.05~-0.02
-0.02~0.02
0.02~0.05
0.05~0.1
0.1~0.2

1026

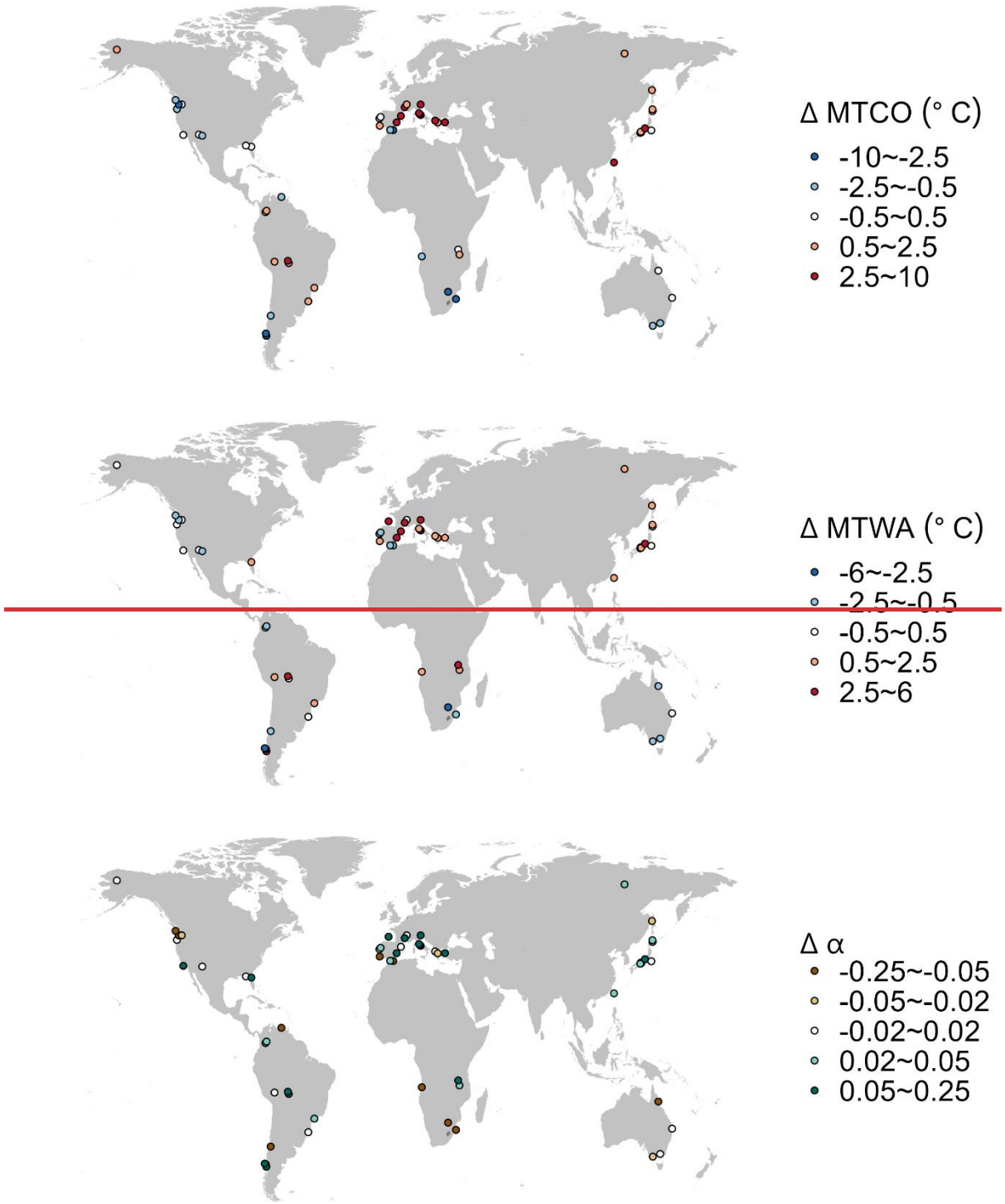

1027

1028

1029

Figure 6: Map showing the change in mean temperature of the coldest month (ΔMTCO) and the change in mean temperature of the warmest month (ΔMTWA) for D-O 9 (a weak event) and D-O 8 (a strong event). The upper panel shows ΔMTCO, while the lower panel shows ΔMTWA.

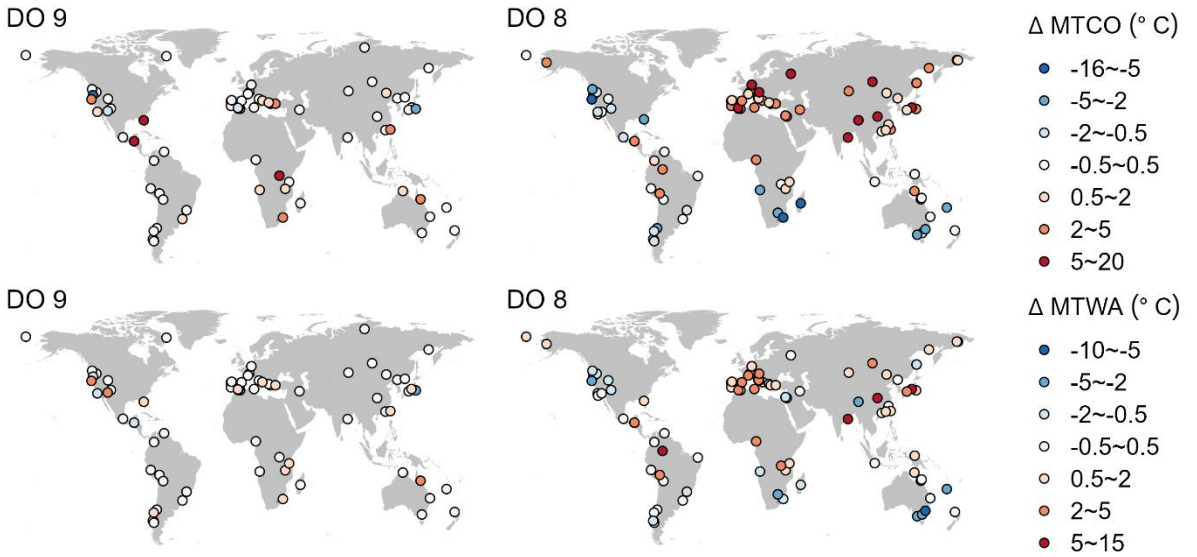

Figure 7: Map showing the median change of LOVECLIM simulations over (ice-free) land for Dansgaard-Oeschger (D-O) events 5 to 12. The upper panel shows the change in mean temperature of the coldest month (ΔMTCO), and the lower panel shows the change in mean temperature of the warmest month (ΔMTWA).

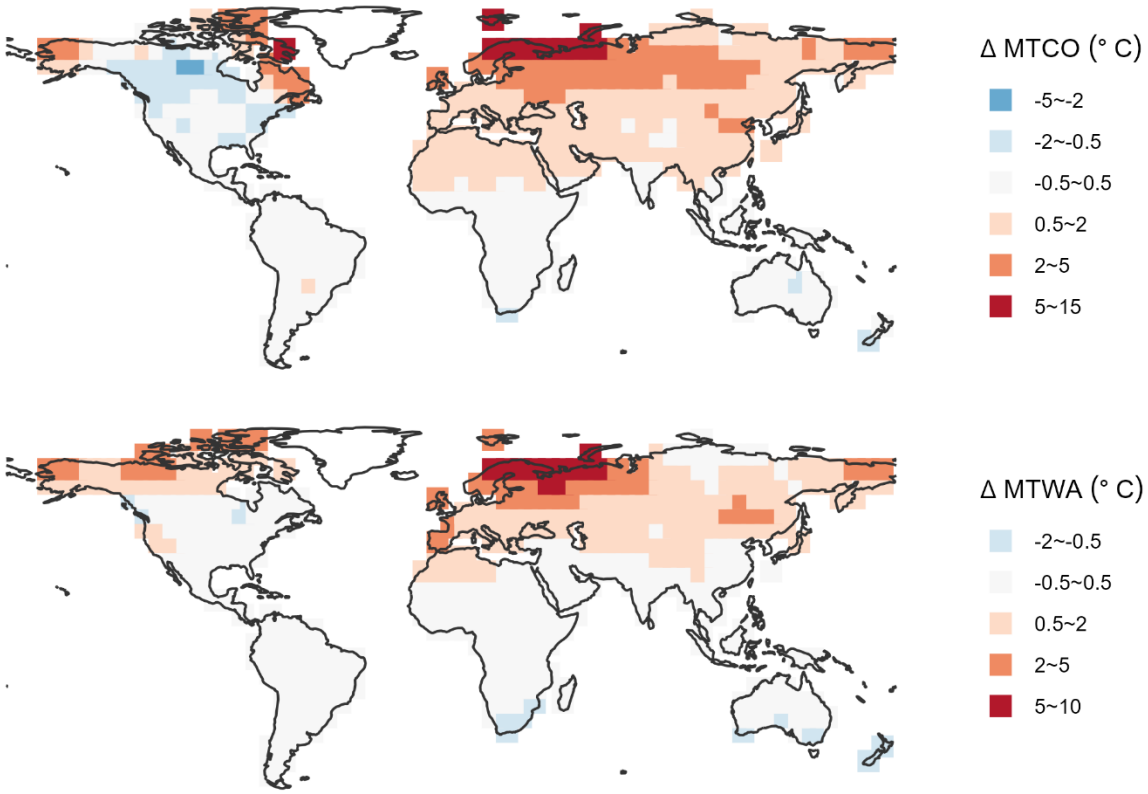

Figure 8: Scatter plot of the change in mean temperature of the coldest month (ΔMTCO) versus the change in mean temperature of the warmest month (ΔMTWA) during individual Dansgaard-Oeschger (D-O) events at individual (ice-free) land grids simulated by the LOVECLIM model, using the same way to identify changes as the reconstructions. The points are grouped into the northern extratropics (NET, north of 23.5°N), the tropics (TROP, between 23.5°N and 23.5°S) and the southern extratropics (SET, south of 23.5°S). The grey lines indicate ± 1 error of the change.

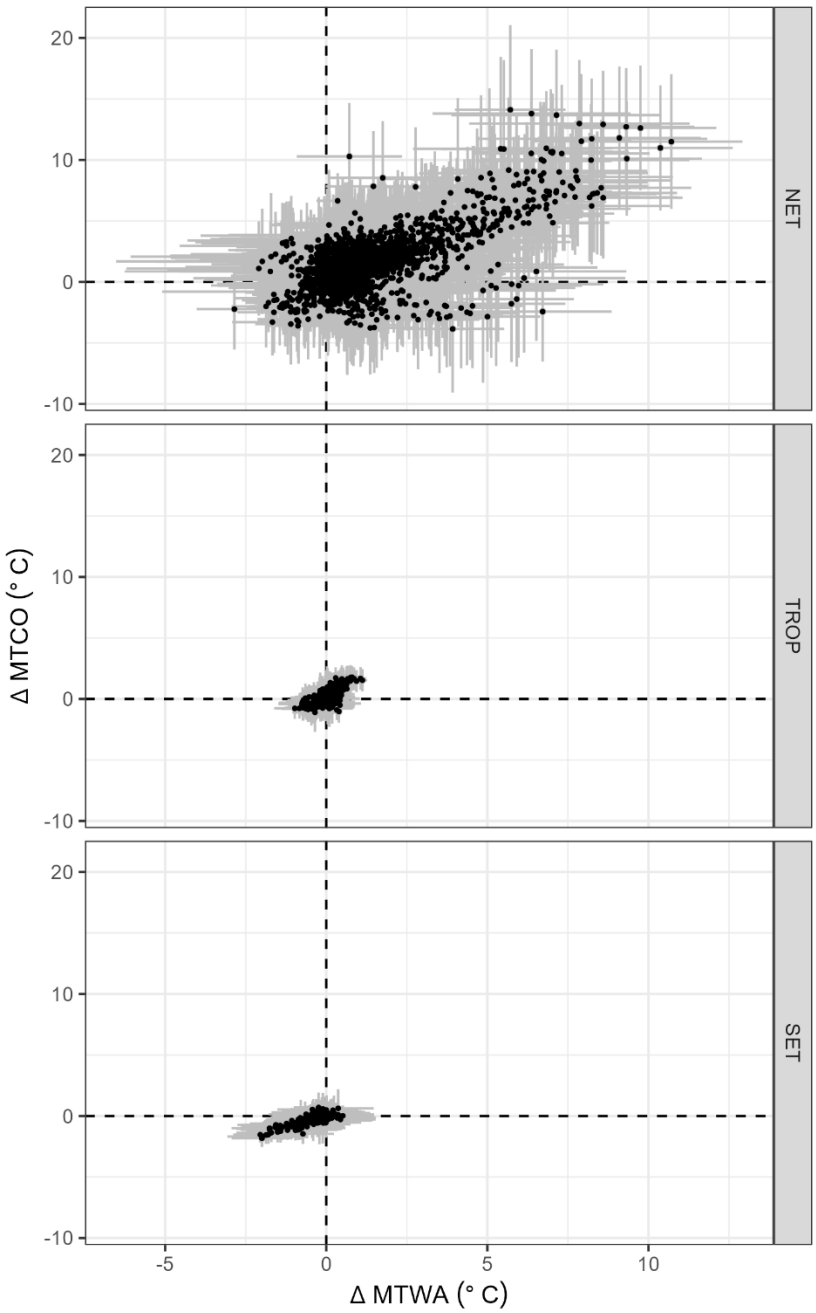

Table 1: ~~Detail~~Site informations of the fossil pollen records ~~sites from the Abrupt Climate Changes and Environmental Responses (ACER) database (Sánchez Goñi et al., 2017)~~ covering the interval ~~between~~ 50~~- ka and~~ 30 ka ~~used for the climate reconstructions~~. The references with full citation are given in Supplementary Materials, section 3. lat is the latitude, lon is the longitude, elv is the elevation (unit: m). TERR means terrestrial record, MARI means marine record. ~~-~~n_{due} is the number of D-O events that should be found based on the time interval covered by the record. n_{miss} is the number of D-O events that were not identified. n_{low} is the number of D-O events missed because of low resolution of that part of the record. Some ~~of the 73~~ sites ~~(indicated by NA in n_{due}, n_{miss} and n_{low})~~ provide records ~~for parts of the~~in 50-30 ka ~~interval~~ but do ~~not for~~not cover the intervals of the D-O events; some marine sites are too far from the land to extract GWR modern MTGR to apply CO_2 correction; these sites are all indicated by NA in n_{due}, n_{miss} and n_{low}. ~~Reconstructions based on samples where the D-O signal was not identified were not used in subsequent analyses. The full citations for each site are given in Supplementary Materials.~~

name	lat	lon	elv	type	source	n_{due}	n_{miss}	n_{low}
Abric Romani	41.53	1.68	350	TERR	ACER	2	0	0
Akulinin Exposure P1282	47.12	138.55	20	TERR	Legacy2	1	0	0
Alut Lake	60.14	152.31	480	TERR	Cao et al. (2019, 2020)	7	1	1
Anderson Pond (ANDERSON)	36.03	−85.50	303	TERR	Legacy2	NA	NA	NA
Auel_AU2	50.28	6.59	457	TERR	AUTHOR	7	0	0
Aueler Maar_ELSA_AU3	50.28	6.60	456	TERR	Pangaea	3	0	0
Aueler Maar_ELSA_AU4	50.28	6.59	457	TERR	Pangaea	7	2	2
Azzano Decimo	45.88	12.72	10	TERR	ACER	4	0	0
Bajondillo	36.62	−4.50	20	TERR	Legacy2	2	0	0
Baldwin Lake	34.28	−116.81	2060	TERR	Legacy2	4	1	1
Balikun Lake	43.68	92.80	1575	TERR	Legacy2	NA	NA	NA
Balikun Lake BLK11A	43.68	92.80	1575	TERR	AUTHOR	2	0	0
Bambili 2	5.93	10.24	2323	TERR	Legacy2	5	1	1
Bandung DPDR-II	−6.99	107.73	662	TERR	Legacy2	4	2	2
Bay of Biscay	45.35	−5.22	−4100	MARI	Legacy2	NA	NA	NA
Bear Lake (BL00-1E)	41.95	−111.31	1805	TERR	ACER	7	2	2
Berelyekh River	63.28	147.75	800	TERR	Cao et al. (2019, 2020)	NA	NA	NA

Biggsville [Cessford Quarry]	40.86	−90.88	198	TERR	Legacy2	1	0	0
Bolotnyii Stream Exposure 117	42.85	132.78	4	TERR	Legacy2	2	1	1
Bolshoe Toko PG2133	56.04	130.87	903	TERR	Legacy2	2	0	0
Bolshoy Lyakhovsky Island	73.33	141.50	7	TERR	Legacy2	NA	NA	NA
Boney Spring	38.11	−93.37	210	TERR	Legacy2	1	1	1
Byllatskoye Exposure, Byllat River, Indigirka Basin	69.17	140.06	316	TERR	Legacy2	NA	NA	NA
Cala Conto	−17.57	−65.93	2700	TERR	Legacy2	2	2	2
Caledonia Fen	−37.33	146.73	1280	TERR	ACER	7	2	2
Cambara do Sul	−29.05	−50.10	1040	TERR	ACER	7	2	0
Camel Lake	30.26	−85.01	20	TERR	ACER	2	1	1
Carp Lake	45.91	−120.88	720	TERR	ACER	8	3	3
Changping CHZK1	40.18	116.22	49	TERR	Zhou et al. (2023)	NA	NA	NA
Chenghai CH2	23.48	116.80	5	TERR	Zhou et al. (2023)	4	1	1
Cheremushka Bog	52.75	108.08	1500	TERR	Cao et al. (2019, 2020)	1	0	0
Colonia	−23.87	−46.71	900	TERR	ACER	7	5	5
Colonia CO3	−23.87	−46.71	900	TERR	Legacy2	7	4	4
Core Trident 163 31B	−3.61	−83.96	−3210	MARI	ACER	NA	NA	NA
Correo	44.56	6.00	1100	TERR	Legacy2	1	0	0
Crystal Lagoon	−40.48	148.35	8	TERR	Legacy2	1	0	0
Daihai Lake-Wajianggou	40.58	112.67	1500	TERR	Zhou et al. (2023)	NA	NA	NA
Dajiu Lake DJH-1	31.49	110.00	1751	TERR	Zhou et al. (2023)	8	1	1
Dalai Nur Lake-Haiyan	43.28	116.58	1200	TERR	Zhou et al. (2023)	NA	NA	NA
Daluoba	47.83	88.20	2020	TERR	Zhou et al. (2023)	NA	NA	NA
Dar Fatma	36.82	8.77	780	TERR	Legacy2	7	2	2
Daxing DZK1	39.72	116.32	49	TERR	Zhou et al. (2023)	NA	NA	NA
Dead Sea	31.51	35.47	−428	TERR	Pangaea	6	0	0
Demyanskoye	59.50	69.50	65	TERR	Cao et al. (2019, 2020)	1	0	0
Deva-Deva	−7.12	37.62	2600	TERR	Legacy2	4	1	1
Diexi Lake	32.04	103.68	2334	TERR	Zhou et al. (2023)	2	0	0
Dikikh Olyenyeii Lake	67.75	−178.83	300	TERR	Cao et al. (2019, 2020)	3	1	1
Eastern Niger Delta	4.55	6.43	0	TERR	Legacy2	NA	NA	NA

Elikchan 4 Lake	60.75	151.88	810	TERR	Cao et al. (2019, 2020)	3	1	1
Emanda	65.29	135.76	671	TERR	Legacy2	4	1	1
Enmynveem River (mammoth site)	68.17	165.93	400	TERR	Legacy2	NA	NA	NA
Enmynveem River1	68.17	165.93	400	TERR	Cao et al. (2019, 2020)	NA	NA	NA
Erlongwan Maar Lake	42.30	126.37	724	TERR	Zhou et al. (2023)	2	0	0
Ershilipu	36.93	116.65	50	TERR	Zhou et al. (2023)	NA	NA	NA
EW9504-17 PC	42.23	−125.81	−2671	MARI	ACER	NA	NA	NA
F2-92-P29	32.90	−119.73	−1475	MARI	ACER	2	2	2
Faddeyevskiy	75.33	143.83	30	TERR	Legacy2	NA	NA	NA
Fargher Lake	45.88	−122.58	200	TERR	ACER	8	2	1
Feng Suancigou Feng	35.51	105.81	1840	TERR	Zhou et al. (2023)	1	1	1
Fog Lake	67.18	−63.25	422	TERR	Legacy2	2	1	1
Fundo Nueva	−41.28	−73.83	66	TERR	ACER	5	1	0
Fuquene	5.45	−73.46	2540	TERR	ACER	7	3	3
Furamoos	47.98	9.88	662	TERR	ACER	NA	NA	NA
Gantang SZY	26.77	119.03	1007	TERR	Zhou et al. (2023)	5	1	1
GeoB2107-3	−27.18	−46.45	−1048	MARI	Legacy2	NA	NA	NA
GeoB3104	−3.67	−37.72	−767	MARI	ACER	1	1	1
Girraween Lagoon	−12.52	131.08	25	TERR	AUTHOR	5	1	1
Goshen Springs	31.72	−86.13	105	TERR	Legacy2	2	2	2
Grass Lake	41.65	−122.17	1537	TERR	Legacy2	3	0	0
Grays Lake (GRAYSGL1)	43.07	−111.44	1195	TERR	Legacy2	4	1	1
Grays Lake (GRAYSGL6)	43.07	−111.44	1195	TERR	Legacy2	NA	NA	NA
Guangzhou GZ-2	22.71	113.51	1	TERR	Zhou et al. (2023)	3	2	2
Guangzhou GZ-4	23.27	113.21	4	TERR	Zhou et al. (2023)	1	0	0
Gytgykai Lake	63.42	176.57	102	TERR	Cao et al. (2019, 2020)	1	0	0
Hachihama	34.55	133.95	6	TERR	Legacy2	3	1	1
Hangzhou HQB7	30.47	120.21	2	TERR	Zhou et al. (2023)	1	0	0
Hay Lake	34.00	−109.43	2780	TERR	ACER	NA	NA	NA
Headwaters Opasnaya River	48.23	138.48	1320	TERR	Legacy2	NA	NA	NA
Hosoike Moor	35.35	134.13	970	TERR	Legacy2	4	2	2
Huguangyan Maar Lake B	21.15	110.28	88	TERR	Zhou et al. (2023)	NA	NA	NA

Huinamarca (Lake Titicaca)	−16.23	−68.77	3810	TERR	ACER	3	0	0
Indigirka lowlands	70.58	145.00	20	TERR	Cao et al. (2019, 2020)	1	0	0
Ioannina	39.75	20.85	470	TERR	ACER	8	1	0
IODP Site 353-U1446A	19.08	85.73	−1430.2	MARI	Pangaea	6	1	1
Iwaya site	35.52	135.89	20	TERR	Legacy2	3	1	1
Jackson Pond (JACKSN07)	37.43	−85.72	260	TERR	Legacy2	NA	NA	NA
Jiangcun	34.40	109.50	650	TERR	Zhou et al. (2023)	3	0	0
Joe Lake	66.77	−157.22	183	TERR	ACER	3	1	1
Julietta Lake	61.34	154.56	880	TERR	Cao et al. (2019, 2020)	3	0	0
Kai Iwa	−35.82	173.65	70	TERR	AUTHOR	6	2	2
Kaiyak Lake	68.14	−161.44	190	TERR	Legacy2	NA	NA	NA
Kalaloch	47.63	−124.38	24	TERR	Legacy2	8	1	0
Kalistratikha	53.33	83.25	190	TERR	Cao et al. (2019, 2020)	NA	NA	NA
Kalistratikha Exposure	53.33	83.25	190	TERR	Legacy2	NA	NA	NA
Kamiyoshi Basin (KY01)	35.10	135.59	335	TERR	ACER	1	0	0
Kashiru Bog	−3.47	29.57	2240	TERR	ACER	NA	NA	NA
Kenbuchi Basin	44.05	142.38	135	TERR	ACER	3	0	0
Khoe	51.34	142.14	15	TERR	ACER	1	0	0
Khoe, Sakhalin Island	51.34	142.14	15	TERR	Cao et al. (2019, 2020)	4	2	2
Kirgirlakh Stream, Berelyekh River Basin (DIMA2)	62.67	147.98	700	TERR	Legacy2	NA	NA	NA
Kirgirlakh Stream, Berelyekh River Basin (DIMA3)	62.67	147.98	700	TERR	Legacy2	1	0	0
Kirgirlakh Stream_2	62.67	147.98	700	TERR	Cao et al. (2019, 2020)	1	1	1
Kohuora	−36.95	174.87	5	TERR	ACER	NA	NA	NA
Komanimambuno Mire	−5.82	145.09	2740	TERR	Legacy2	NA	NA	NA
Kunming Basin KZ2-3	25.00	102.62	1890	TERR	Zhou et al. (2023)	NA	NA	NA
Kupena (KUPENA3)	41.98	24.33	1356	TERR	Legacy2	NA	NA	NA
Kurota Lowland	35.52	135.88	20	TERR	ACER	1	0	0
KW31	3.52	5.57	−1181	MARI	ACER	1	0	0
La Laguna	4.92	−74.03	2900	TERR	ACER	1	0	0
Labaz lake (LAO6-95)	72.29	99.61	42	TERR	Legacy2	2	1	0

Lac du Bouchet - DIGI	44.83	3.82	1200	TERR	ACER	8	1	0
Lac Emeric	−22.30	166.97	230	TERR	Legacy2	3	1	1
Lac Suprin	−22.29	166.99	235	TERR	Legacy2	4	2	2
Lagaccione	42.57	11.80	355	TERR	ACER	3	0	0
Lago Grande di Monticchio	40.94	15.61	656	TERR	ACER	8	0	0
Lagoa Campestre de Salitre (SALILC3)	−19.00	−46.77	980	TERR	Legacy2	3	2	2
Lagoa das Patas	0.27	−66.68	300	TERR	Legacy2	4	1	1
Laguna Bella Vista	−13.62	−61.55	600	TERR	ACER	2	1	1
Laguna Chaplin	−14.47	−61.07	600	TERR	ACER	NA	NA	NA
Laguna Ciega	6.48	−72.39	3510	TERR	Legacy2	NA	NA	NA
Laguna Junin	−11.00	−76.17	4100	TERR	Legacy2	5	2	2
Lake Ailike	46.54	86.36	278	TERR	AUTHOR	5	0	0
Lake Albert (Lake Mobutu Sese Seko)	1.83	31.17	619	TERR	Legacy2	NA	NA	NA
Lake Annie	27.21	−81.35	34	TERR	Legacy2	1	0	0
Lake Baikal_BDP99	52.09	105.84	456	TERR	Pangaea	7	0	0
Lake Billyakh	65.28	126.78	340	TERR	ACER	3	0	0
Lake Biwa (BIW95-4)	35.25	136.05	84	TERR	ACER	3	0	0
Lake Carpentaria	−12.52	140.35	−60	MARI	Legacy2	4	2	2
Lake Chalco CHA08	19.25	−98.97	2250	TERR	AUTHOR	5	1	1
Lake Consuelo (CON1)	−13.95	−68.99	1360	TERR	ACER	7	2	2
Lake E5	68.64	−149.46	803	TERR	Legacy2	NA	NA	NA
Lake Elsinore	33.66	−117.35	376	TERR	Legacy2	1	0	0
Lake Fimon	45.47	11.53	23	TERR	AUTHOR	NA	NA	NA
Lake George	−35.09	149.43	673	TERR	Legacy2	4	0	0
Lake Hordorli	−2.54	140.59	798	TERR	Legacy2	4	0	0
Lake Iznik	40.43	29.53	88	TERR	Legacy2	1	0	0
Lake Malawi	−11.22	34.42	470	TERR	ACER	5	2	2
Lake Masoko	−9.33	33.75	840	TERR	ACER	2	1	1
Lake Nero (NERO2)	57.18	39.45	93	TERR	Legacy2	NA	NA	NA
Lake Nojiri	36.83	138.22	657	TERR	ACER	8	0	0
Lake Patzcuaro	19.58	−101.58	2044	TERR	Legacy2	2	1	1
Lake Peten-Itza	16.99	−89.82	110	TERR	Legacy2	8	1	1
Lake Quexil	16.92	−89.82	110	TERR	Legacy2	4	2	2
Lake Selina	−41.88	145.61	516	TERR	Legacy2	1	0	0
Lake Tanganyika (KH3)	−8.50	30.75	773	TERR	Legacy2	4	2	2
Lake Tanganyika (KH4)	−8.50	30.75	773	TERR	Legacy2	NA	NA	NA
Lake Tanganyika [north basin] (SD24TAN)	−4.19	29.31	773	TERR	Legacy2	NA	NA	NA
Lake Tritrivakely	−19.78	46.92	1778	TERR	Legacy2	5	1	0
Lake Tulane	29.83	−81.95	36	TERR	ACER	7	1	1
Lake Wangoom LW87 core	−38.35	142.60	100	TERR	ACER	4	0	0

Lake Xinias	39.05	22.27	500	TERR	ACER	8	3	3
Lake Yamozero	65.02	50.23	213	TERR	Legacy2	2	0	0
Lake Zeribar	35.53	46.12	1288	TERR	Legacy2	7	1	1
Ledovyi Obryv Exposure, Northern Section	64.10	171.18	57	TERR	Legacy2	NA	NA	NA
Les Echets G - DIGI	45.90	4.93	267	TERR	ACER	8	0	0
Levantine Basin	32.03	34.28	0	TERR	Legacy2	4	1	1
Levinson Lessing Lake PG1228	74.47	98.64	47	TERR	Cao et al. (2019, 2020)	1	0	0
Little Lake	44.16	−123.58	217	TERR	ACER	5	0	0
Lop Nur K1	40.28	90.25	780	TERR	Zhou et al. (2023)	NA	NA	NA
Luanhaizi Lake LH2	37.59	101.35	3200	TERR	Zhou et al. (2023)	1	0	0
Luochuan	35.75	109.42	1068	TERR	Zhou et al. (2023)	NA	NA	NA
Lynchs Crater	−17.37	145.70	760	TERR	ACER	7	4	4
Malyi Krechet Lake	64.80	175.53	32	TERR	Legacy2	2	0	0
Mamontovy Khayata	71.77	129.45	0	TERR	Cao et al. (2019, 2020)	3	0	0
Mamontovy Klyk	73.61	117.13	25	TERR	Legacy2	1	0	0
MD01-2421	36.02	141.77	−2224	MARI	ACER	8	1	0
MD03-2622 Cariaco Basin	10.71	−65.17	−877	MARI	ACER	7	5	3
MD04-2845	45.35	−5.22	−4100	MARI	ACER	NA	NA	NA
MD84-629	32.07	34.35	−745	MARI	ACER	5	1	1
MD95-2039	40.58	−10.35	−3381	MARI	ACER	8	1	1
MD95-2042	37.80	−10.17	−3148	MARI	ACER	8	1	1
MD95-2043	36.14	−2.62	−1841	MARI	ACER	8	1	1
MD99-2331	41.15	−9.68	−2110	MARI	ACER	7	1	1
Megali Limni	39.10	26.32	323	TERR	ACER	6	0	0
Melkoye Lake	64.86	175.23	36	TERR	Cao et al. (2019, 2020)	1	0	0
Mereya River	46.62	142.92	4	TERR	Cao et al. (2019, 2020)	NA	NA	NA
Mfabeni Peatland	−28.15	32.52	11	TERR	ACER	4	1	0
Middle Butte Cave	43.37	−112.62	1590	TERR	Legacy2	NA	NA	NA
Milin	29.31	94.35	2982	TERR	Zhou et al. (2023)	3	0	0
Moershoofd	51.25	3.52	2	TERR	Legacy2	NA	NA	NA
Morro de Itapeva	−22.78	−45.53	1850	TERR	Legacy2	NA	NA	NA
Mud Lake (MUDLAKE)	29.30	−81.87	9	TERR	Legacy2	4	1	1
Muscotah Marsh	39.53	−95.51	280	TERR	Legacy2	NA	NA	NA
Nachtigall	51.81	9.40	95	TERR	Legacy2	NA	NA	NA

Nakafurano	43.37	142.43	173	TERR	ACER	2	1	1
Native Companion Lagoon	−27.68	153.41	20	TERR	ACER	4	2	2
Navarres	39.10	−0.68	225	TERR	ACER	3	0	0
Ngamakala Pound (GAMA4)	−4.08	15.38	400	TERR	Legacy2	NA	NA	NA
Ngoring Lake CK6	34.92	97.73	4272	TERR	Zhou et al. (2023)	NA	NA	NA
Noordzee T121	54.10	4.21	0	TERR	Legacy2	NA	NA	NA
Northern Coast of Onemen Gulf	64.78	176.17	18	TERR	Legacy2	3	0	0
ODP 1233 C	−41.00	−74.45	−838	MARI	ACER	8	2	1
ODP 1234	−36.22	−73.68	−1015	MARI	ACER	8	0	0
ODP 820	−16.63	146.30	−280	MARI	ACER	5	3	3
ODP site 976	36.20	−4.30	−1108	MARI	ACER	8	1	0
ODP1019	41.66	−124.91	989	MARI	ACER	7	3	3
ODP1078C	−11.92	13.40	−426	MARI	ACER	8	2	1
ODP893A	34.28	−120.03	−577	MARI	ACER	8	0	0
Oil Lake	70.29	−151.17	745	TERR	Legacy2	2	0	0
Okarito Pakihi	−43.24	170.22	70	TERR	ACER	NA	NA	NA
Ovrazhnyi Stream-2	43.25	134.57	10	TERR	Cao et al. (2019, 2020)	NA	NA	NA
Ovrazhnyii-1 Stream Exposure	43.25	134.57	8	TERR	Legacy2	NA	NA	NA
Ovrazhnyii-2 Exposure 667-842	43.25	134.57	10	TERR	Legacy2	NA	NA	NA
Padul	37.01	−3.60	726	TERR	AUTHOR	6	2	2
Paramonovskii Stream	43.20	133.75	120	TERR	Cao et al. (2019, 2020)	NA	NA	NA
Paramonovskii Stream Exposure 4980	43.20	133.75	120	TERR	Legacy2	NA	NA	NA
Pavlovka Exposure 988	44.32	134.00	300	TERR	Legacy2	NA	NA	NA
Peloncillo Mountains	32.29	−109.09	1400	TERR	Legacy2	NA	NA	NA
Peschanka Exposure 155	43.30	132.12	12	TERR	Legacy2	NA	NA	NA
Pittsburg Basin	38.90	−89.19	162	TERR	Legacy2	NA	NA	NA
Plesheevo Lake	56.77	38.78	148	TERR	Legacy2	2	0	0
Potato Lake	34.45	−111.33	2222	TERR	ACER	1	1	1
Poutu	−36.38	174.13	82	TERR	AUTHOR	1	1	1
Pretoria Saltpan	−25.41	28.08	1150	TERR	Legacy2	4	0	0
Qingdao ZK2	36.29	120.46	31	TERR	Zhou et al. (2023)	NA	NA	NA
Qingdao ZK3	36.26	120.64	7	TERR	Zhou et al. (2023)	NA	NA	NA
Rahue	−39.37	−70.93	1000	TERR	Legacy2	NA	NA	NA
Reenadinna Wood	52.01	−9.53	20	TERR	Legacy2	NA	NA	NA

Rice Lake (Rice Lake 81)	40.30	−123.22	1100	TERR	ACER	NA	NA	NA
Rietvlei-Still Bay	−34.35	21.54	17	TERR	Legacy2	NA	NA	NA
Rio Timbio	2.37	−76.71	1750	TERR	Legacy2	NA	NA	NA
Rockyhock Bay	36.17	−76.68	6	TERR	Legacy2	NA	NA	NA
Ruby Marsh	41.13	−115.51	1818	TERR	Legacy2	1	0	0
Rusaka Swamp	−3.43	29.62	2070	TERR	Legacy2	1	0	0
Sacred Lake	0.05	37.53	2345	TERR	Legacy2	3	2	2
Saint-Ursin	48.52	−0.25	234	TERR	Legacy2	3	0	0
San Agustin Plains (SAPBHM)	33.87	−108.25	2069	TERR	Legacy2	NA	NA	NA
Sangluoshu	37.50	117.73	50	TERR	Zhou et al. (2023)	NA	NA	NA
Sanshui K5	22.78	112.63	12	TERR	Zhou et al. (2023)	NA	NA	NA
Shaamar	50.20	105.20	650	TERR	Legacy2	2	0	0
Shuidonggou SDG2	38.28	106.50	1200	TERR	Zhou et al. (2023)	NA	NA	NA
Shunyi GZK1	40.15	116.53	50	TERR	Zhou et al. (2023)	NA	NA	NA
Siberia	−17.09	−64.72	2920	TERR	ACER	1	1	1
Siberia1	−17.09	−64.72	2920	TERR	Legacy2	1	1	1
Sihailongwan Maar Lake	42.28	126.60	797	TERR	Pangaea	8	1	1
Siluyanov Yar-2 Exposure	46.13	137.83	25	TERR	Legacy2	NA	NA	NA
Sirunki Wabag	−5.44	143.53	2550	TERR	Legacy2	2	0	0
St. Catherines Island (Northwest Marsh)	31.69	−81.15	0	TERR	Legacy2	NA	NA	NA
Stoneman Lake_STL	34.78	−111.52	2048	TERR	AUTHOR	3	0	0
Stracciacappa	42.13	12.32	220	TERR	ACER	4	0	0
Straldzha mire (QUARRY)	42.63	26.78	137	TERR	Legacy2	NA	NA	NA
Tagua Tagua - DIGI	−34.50	−71.16	200	TERR	ACER	6	1	1
Taiquemo	−42.17	−73.60	170	TERR	ACER	8	0	0
Tanon River	59.67	151.20	40	TERR	Cao et al. (2019, 2020)	NA	NA	NA
Tanon River [Quarry Site]	59.67	151.20	40	TERR	Legacy2	NA	NA	NA
Taymyr Lake SAO1	74.55	100.53	47	TERR	Cao et al. (2019, 2020)	NA	NA	NA
Tianshuihai TS95	35.35	79.52	4900	TERR	Zhou et al. (2023)	1	0	0
Tianyang Maar Lake TYC	20.52	110.30	108	TERR	Zhou et al. (2023)	3	0	0
Tianyang TY1	20.35	110.35	90	TERR	Zhou et al. (2023)	1	1	0
Tikhangou Exposure	42.83	132.78	4	TERR	Legacy2	NA	NA	NA

Toadlena Lake [Dead Man Lake] (DEAD5826)	36.24	−108.95	2759	TERR	Legacy2	1	0	0
Toadlena Lake [Dead Man Lake] (DEAD6101)	36.24	−108.95	2759	TERR	Legacy2	4	2	2
Tortoise Lagoon	−27.52	153.47	39	TERR	Legacy2	2	2	2
Toushe Basin	23.82	120.88	650	TERR	ACER	8	0	0
Toushe Lake 2013	23.82	120.88	650	TERR	Zhou et al. (2023)	1	0	0
Tswaing Crater	−25.40	28.08	1100	TERR	ACER	5	0	0
Tukuto Lake	68.50	−157.03	505	TERR	Legacy2	1	1	1
Tyrrendara Swamp	−38.20	141.76	13	TERR	ACER	NA	NA	NA
Ulan Buh Desert WL10ZK-1	40.04	105.78	1026	TERR	Zhou et al. (2023)	NA	NA	NA
Valle di Castiglione	41.90	12.76	44	TERR	ACER	7	3	3
Villarquemado	40.82	−1.48	985	TERR	AUTHOR	4	1	0
Vinillos	−0.60	−77.85	2090	TERR	Legacy2	1	0	0
Voordrag	−27.74	31.33	940	TERR	Legacy2	NA	NA	NA
W8709-13 PC	42.11	−125.75	−2712	MARI	ACER	NA	NA	NA
W8709-8 PC	42.26	−127.68	−3111	MARI	ACER	NA	NA	NA
Walker Lake	35.38	−111.71	2500	TERR	ACER	NA	NA	NA
Wenquangou	35.92	94.20	4700	TERR	Zhou et al. (2023)	NA	NA	NA
White Pond (WHITESC)	34.17	−80.78	90	TERR	Legacy2	NA	NA	NA
Wulagai Lake	45.42	117.48	822	TERR	AUTHOR	7	0	0
Xere Wapo	−22.30	166.96	235	TERR	Legacy2	NA	NA	NA
Xijir Ulan Lake	35.23	90.33	4500	TERR	Zhou et al. (2023)	NA	NA	NA
Xining ZK2	35.97	101.67	4363	TERR	Zhou et al. (2023)	NA	NA	NA
Yabulai Mt	39.62	103.92	1266	TERR	Zhou et al. (2023)	2	0	0
Yangerzhuang	38.35	117.35	5	TERR	Zhou et al. (2023)	NA	NA	NA
Yangjiapo	40.02	118.68	70	TERR	Zhou et al. (2023)	NA	NA	NA
Yangyuan-Caocun	40.10	114.40	875	TERR	Zhou et al. (2023)	1	0	0
Yaxi Co Lake	34.28	92.67	4000	TERR	Zhou et al. (2023)	NA	NA	NA
Zagoskin Lake	63.45	−162.11	7	TERR	Legacy2	5	0	0
Zhongshan PK19	21.80	113.30	6	TERR	Zhou et al. (2023)	NA	NA	NA

~~Site name~~	~~Latitude~~	~~Longitude~~	~~Elevation (m)~~	~~Reference(s)~~	~~n_{due}~~	~~n_{miss}~~	~~n_{low}~~
~~Abric Romanì~~	~~41.53~~	~~1.68~~	~~350~~	~~Burjachs & Julià (1994)~~	~~2~~	~~0~~	~~0~~
~~Azzano Decimo~~	~~45.8833~~	~~12.7165~~	~~10~~	~~Pini et al. (2009)~~	~~6~~	~~2~~	~~2~~

Caledonia Fen	-37.3333	146.7333	1280	Kershaw et al. (2007b)	8	0	0
Cambara do Sul	-29.05	-50.1	1040	Behling et al. (2004)	7	0	0
Camel Lake	30.26	-85.01	20	Watts et al. (1992)	2	1	1
Carp Lake	45.91	-120.88	720	Whitlock and Bartlein (1997); Whitlock et al. (2000)	8	1	1
Colônia	-23.87	-46.71	900	Ledru et al. (2009)	7	2	2
Core Trident 163 31B	-3.61	-83.96	-3210	Heusser and Shackleton (1994)	NA	NA	NA
Fargher Lake	45.88	-122.58	200	Grigg and Whitlock (2002)	8	2	1
Fundo Nueva	-41.28	-73.83	66	Heusser et al. (2000)	6	1	0
Fuquene	5.45	-73.46	2540	van Geel and van der Hammen (1973); Mommerstseeg (1998)	7	3	3
Füramoos	47.98	9.88	662	Müller et al. (2003)	NA	NA	NA
GeoB3104	-3.67	-37.72	-767	Behling et al. (2000)	NA	NA	NA
Hay Lake	34	-109.425	2780	Jacobs (1985)	5	3	3
Ioannina	39.75	20.85	470	Tzedakis et al. (2002); Tzedakis et al. (2004)	8	1	0
Joe Lake	66.76667	-157.217	183	Anderson (1988); Anderson et al. (1994)	7	3	3
Kalaloch	47.6053	-124.371	19	Heusser (1972)	8	1	0
Kamiyoshi Basin (KY01)	35.102	135.586	335	Takahara et al. (2000); Takahara et al. (2007); Hayashi et al. (2009)	2	0	0
Kashiru Bog	-3.47	29.57	2240	Bonnefille & Riollet (1988); Bonnefille et al. (1992)	2	2	2
Kenbuchi Basin	44.05	142.383	135	Igarashi et al. (1993);	3	0	0

				Igarashi (1996)			
Khoe	51.341	142.14	15	Igarashi et al. (2002)	6	2	2
Kohuora	-36.95	174.8667	5	Newnham et al. (2007)	NA	NA	NA
Kurota Lowland	35.517	135.879	20	Takahara & Kitagawa (2000)	3	0	0
KW31	3.52	5.57	-1181	Lézine & Cazet (2005); Lézine et al. (2005)	NA	NA	NA
La Laguna	4.92	-74.03	2900	Helmens et al., 1(996)	2	0	0
Lac du Bouchet	44.83	3.82	1200	Reille and de Beaulieu (1990)	8	0	0
Lagaccione	42.57	11.8	355	Magri (1999); Magri (2008)	7	0	0
Laguna Bella Vista	-13.6167	-61.55	600	Burbridge et al. (2004)	2	0	0
Laguna Chaplin	-14.4667	-61.0667	600	Burbridge et al. (2004)	3	0	0
Lake Billyakh	65.2833	126.7833	340	Müller et al. (2010)	4	0	0
Lake Biwa (BIW95-4)	35.245	136.054	84	Takemura et al. (2000); Hayashida et al. (2007); Hayashi et al. (2010)	3	0	0
Lake Consuelo (CON1)	-13.95	-68.991	1360	Urrego et al. (2005); Urrego et al. (2010)	7	0	0
Lake Malawi	-11.22	34.42	470	DeBusk (1998)	6	1	1
Lake Masoko	-9.33	33.75	840	Vincens et al. (2007)	2	0	0
Lake Nojiri	36.831	138.216	657	Kumon et al. (2009)	8	0	0
Lake Tulane	29.83	-81.95	36	Grimm et al. (1993); Grimm et al. (2006)	8	2	2
Lake Wangoom LW87 core	-38.35	142.6	100	Harle et al. (2002)	7	1	1
Lake Xinias	39.05	22.27	500	Bottema (1979)	8	3	3

Les Echets G	45.9	4.93	267	de Beaulieu & Reille (1984)	8	1	0
Little Lake	44.16	-123.58	217	Grigg et al. (2001)	5	0	0
Lynchs Crater	-17.3667	145.7	760	Kershaw et al. (2007a)	8	1	1
MD01-2421	36.02	141.77	-2224	Igarashi & Oba (2006); Oba et al. (2006); Aoki et al. (2008)	8	0	0
MD03-2622 Cariaco Basin	10.7061	-65.1691	-877	González et al. (2008); González and Dupont (2009)	3	0	0
MD04-2845	45.35	-5.22	-4100	Sánchez Goñi et al. (2008); Daniau et al. (2009)	2	0	0
MD84-629	32.07	34.35	-745	Cheddadi & Rossignol-Strick (1995)	NA	NA	NA
MD95-2039	40.58	-10.35	-3381	Roucoux et al. (2001); Roucoux et al. (2005)	5	0	0
MD95-2042	37.8	-10.17	-3148	Sánchez Goñi et al. (1999); Sánchez Goñi et al. (2000); Daniau et al. (2007); Sánchez Goñi et al. (2008); (Sánchez Goñi et al. (2009)	6	0	0
MD95-2043	36.14	-2.621	-1841	Sánchez Goñi et al. (2002); Fletcher and Sánchez Goñi (2008)	4	0	0
MD99-2331	41.15	-9.68	-2110	Sánchez Goñi et al. (2005); Naughton et al.	5	0	0

				(2007); Sánchez Goñi et al. (2008); Naughton et al. (2009)			
Megali Limni	39.1025	26.3208	323	Margari et al. (2007); Margari et al. (2009)	6	0	0
Mfabeni Peatland	-28.1487	32.51867	11	Finch & Hill (2008)	5	1	0
Nakafurano	43.367	142.433	173	Igarashi et al. (1993)	2	0	0
Native Companion Lagoon	-27.68	153.41	20	Petherick et al. (2008a); Petherick et al. (2008b)	6	0	0
Navarrés	39.1	-0.68	225	Carrión & van Geel (1999)	3	0	0
ODP 1233 C	-41	-74.45	-838	Lamy et al. (2004); Heusser et al. (2006)	6	0	0
ODP 820	-16.63	146.3	-280	Moss & Kershaw (2000); Moss & Kershaw (2007)	NA	NA	NA
ODP site 976	36.2	-4.3	-1108	Nebout et al. (2002); Masson-Delmotte et al. (2005)	7	0	0
ODP1019	41.66	-124.91	989	Mix et al. (1999); Pisias et al. (2001)	NA	NA	NA
ODP1078C	-11.92	13.4	-426	Dupont & Behling (2006); Dupont et al. (2008)	8	0	0
ODP893A	34.28	-120.03	-577	Heusser (1998); Heusser (2000)	6	0	0
Potato Lake	34.45	-111.33	2222	Anderson (1993)	4	3	3
Rice Lake (Rice Lake 81)	40.3	-123.22	1100	L. Heusser, unpublished data	NA	NA	NA
Siberia	-17.09	-64.72	2920	Mourguiart & Ledru (2003)	1	1	1

Stracciacappa	42.13	12.32	220	Giardini (2007)	5	1	1
Tagua Tagua	-34.5	-71.16	200	Heusser (1990)	6	0	0
Taiquemo	-42.17	-73.6	170	Heusser et al. (1999); Heusser and Heusser (2006)	8	0	0
Toushe Basin	23.82	120.88	650	Liew et al. (2006)	8	1	1
Tswaing Crater	-25.4	28.08	1100	Partridge et al. (1997); Scott et al. (2008); L. Scott, unpublished data;	6	1	1
Tyrrendara Swamp	-38.1986	141.7626	13	Builth et al. (2008)	NA	NA	NA
Valle di Castiglione	41.9	12.76	44	Alessio et al. (1986); Follieri et al. (1988); Follieri et al. (1989); Narcisi et al. (1992); Narcisi (1999); Magri & Tzedakis (2000); Magri (2008)	7	2	2
W8709-13 PC	42.11	-125.75	-2712	Pisias et al. (2001)	NA	NA	NA
W8709-8 PC	42.26	-127.68	-3111	Heusser (1998); Lyle et al. (1992)	NA	NA	NA
Walker Lake	35.38	-111.71	2500	Berry et al. (1982); Adam et al. (1985); Hevly (1985)	NA	NA	NA

1067

1068

Table 2: Leave-out cross-validation (with geographically and climatically close sites removed) using fxTWA-PLSv2, for mean temperature of the coldest month (MTCO), mean temperature of the warmest month (MTWA) and plant-available moisturewater (αplantα) with P-splines smoothed *fx* estimation and bins of 0.02, 0.02 and 0.002, respectively. P-splines smoothed *fx* was estimated using 200 bins. *n* is the number of components used; Avg.bias is the average bias; RMSEP is the root-mean-square error of prediction; ΔRMSEP% is the per cent change of RMSEP of the current number of components compared to using one component less, i.e. 100 × (RMSEP$_n$ − RMSEP$_{n-1}$) / RMSEP$_{n-1}$. The *p* value assesses whether using the current number of components represents a significant ($p \leq 0.01$) difference over using one fewer component. To avoid over-fitting, the last significant number of components (i.e. the first insignificant number of components minus 1; *p* can become significant again after being insignificant with increasing *n*, but regarded meaningless) is selected for subsequent analyses and indicated in **bold**. The degree of overall compression is assessed by linear regression of the cross-validated reconstructions against the variable; b_1 and σ_{b1} are the slope and the standard error of the slope, respectively. A slope (b_1) of 1 indicates no compression. *n* is the number of components where the last significant number of components is indicated in **bold** (using criteria of $p \leq 0.01$). Avg.bias is the average bias; RMSEP is the root-mean-square error of prediction; and ΔRMSEP is the per cent change of RMSEP, which is 100 × (RMSEP$_n$ − RMSEP$_{n-1}$)/RMSEP$_{n-1}$; when $n = 1$, RMSEP$_0$ is the RMSEP of the null model. *p* assesses whether using the current number of components is significantly different from using one component less. The degree of overall compression is assessed by linear regression of the cross-validated reconstructions on to the climate variable; b_1 and b_1.se are the slope and the standard error of the slope, respectively. The closer the slope (b_1) is to 1, the less the compression.

	n	R^2	Avg.biass	RMSEP	ΔRMSEP%	*p*	b_1	σ_{b1}B*l*.*s*
MTCO (°C)	1	0.720.7	−1.15−1.15	6.896.84	NA−45.20	NA0.001	0.820.8	0.000.0
	2	0.730.7	−1.25−1.24	6.756.68	−2.00−2.38	0.0010.0	0.830.8	0.000.0
	3	**0.740.7**	**−1.20−1.11**	**6.666.52**	**−1.42−2.37**	**0.0010.0**	**0.840.8**	**0.000.0**
	4	0.740.7	−1.23−1.12	6.666.54	0.020.33	0.6630.9	0.840.8	0.000.0
	5	0.74	−1.24	6.64	−0.31	0.001	0.84	0.00
	5	0.740.7	−1.24−1.14	6.636.52	−0.11−0.29	0.0010.0	0.840.8	0.000.0
MTWA (°C)	1	0.510.5	−0.32−0.29	4.004.00	NA−27.76	NA0.001	0.640.6	0.000.0
	2	0.590.6	−0.22−0.20	3.673.62	−8.32−9.42	0.0010.0	0.720.7	0.000.0
	3	**0.600.6**	**−0.25−0.23**	**3.633.58**	**−0.95−1.11**	**0.0010.0**	**0.720.7**	**0.000.0**

	4	0.600.6	−0.25−0.23	3.623.58	−0.290.01	0.0120.5	0.720.7	0.000.0
	5	0.60	−0.27	3.63	0.22	0.974	0.72	0.00
	6	0.600.6	−0.28−0.24	3.613.58	−0.61−0.14	0.0010.0	0.720.7	0.000.0
α_{plant}	1	0.610.6	−0.020−0.0	0.1910.1	NA−37.32	NA0.001	0.650.6	0.000.0
	2	0.620.6	−0.022−0.0	0.1900.1	−0.49−0.61	0.0010.0	0.670.6	0.000.0
	3	**0.630.6**	**−0.020−0.0**	**0.1860.1**	**−2.07−1.18**	**0.0010.0**	**0.680.6**	**0.000.0**
	4	0.64	−0.020	0.186	−0.30	0.020	0.69	0.00
	5	0.640.6	−0.020−0.0	0.1850.1	−0.18−1.46	0.0030.0	0.700.7	0.000.0
	6	0.640.6	−0.020−0.0	0.1850.1	0.09−0.12	0.9880.0	0.700.7	0.000.0

Table 3: Maximum likelihood estimates of the relationship between the change in mean temperature of the coldest month (ΔMTCO) and the change in mean temperature of the warmest month (ΔMTWA) ~~by latitudinal bands~~ for the northern extratropics (NET, north of 23.5°N), tropics (TROP, between 23.5°N and 23.5°S) and southern extratropics (SET, south of 23.5°S). The intercepts were set to zero since both variables are changes.

Region		Coefficient	Standard error (SE)	Lower 95%	Upper 95%
NET	Slope	2.9~~2.135~~	0.5~~0.235~~	2.0~~1.674~~	3.8~~2.596~~
TROP	Slope	2.1~~1.385~~	0.4~~0.753~~	1.2~~=0.091~~	3.0~~2.861~~
SET	Slope	1.5~~1.809~~	0.7~~0.552~~	0.2~~0.728~~	2.8~~2.891~~

Table 4: Maximum likelihood estimates of the relationship between the change in CO_2-corrected plant-available ~~water~~ moisture ($\Delta\alpha_{plant,corrected}$~~$\alpha$~~) and the change in mean temperature of the warmest month (ΔMTWA) ~~by latitudinal bands~~ for the northern extratropics (NET, north of 23.5°N), tropics (TROP, between 23.5°N and 23.5°S) and southern extratropics (SET, south of 23.5°S). The intercepts were set to zero since both variables are changes.

Region		Coefficient	Standard error (SE)	Lower 95%	Upper 95%
NET	Slope	0.27~~0.065~~	0.24~~0.009~~	−0.21~~0.047~~	0.74~~0.082~~
TROP	Slope	0.02~~0.056~~	0.01~~0.009~~	0.01~~0.039~~	0.04~~0.074~~
SET	Slope	−0.03~~0.052~~	0.02~~0.011~~	−0.06~~0.031~~	0.01~~0.073~~

Table 5: Maximum likelihood estimates of the relationship between the change in mean temperature of the coldest month (ΔMTCO) and the change in mean temperature of the warmest month (ΔMTWA) over (ice-free) land in LOVECLIM simulations, for the northern extratropics (NET, north of 23.5°N), tropics (TROP, between 23.5°N and 23.5°S) and southern extratropics (SET, south of 23.5°S). The intercepts were set to zero since both variables are changes.

Region		Coefficient	Standard error (SE)	Lower 95%	Upper 95%
NET	Slope	1.15	0.02	1.11	1.2
TROP	Slope	1.34	0.05	1.25	1.44
SET	Slope	0.76	0.03	0.70	0.81